

The Chiral Potts Models Revisited

Helen Au-Yang and Jacques H.H. Perk^{1,2}

Abstract:

In honor of Onsager's ninetieth birthday, we like to review some exact results obtained so far in the chiral Potts models and to translate these results into language more transparent to physicists, so that experts in Monte Carlo calculations, high and low temperature expansions, and various other methods, can use them.

We shall pay special attention to the interfacial tension ϵ_r between the k state and the $k-r$ state. By examining the ground states, it is seen that the integrable line ends at a superwetting point, on which the relation $\epsilon_r = r \epsilon_1$ is satisfied, so that it is energetically neutral to have one interface or more. We present also some partial results on the meaning of the integrable line for low temperatures where it lives in the non-wet regime. We make Baxter's exact results more explicit for the symmetric case. By performing a Bethe Ansatz calculation with open boundary conditions we confirm a dilogarithm identity for the low-temperature expansion which may be new.

We propose a new model for numerical studies. This model has only two variables and exhibits commensurate and incommensurate phase transitions and wetting transitions near zero temperature. It appears to be not integrable, except at one point, and at each temperature there is a point, where it is almost identical with the integrable chiral Potts model.

KEY WORDS: Chiral Potts model; chiral clock model; star-triangle equations; Yang-Baxter equations; interfacial tension; wetting; superwetting; scaling; corrections to scaling; low-temperature expansions; dilogarithms; Bethe Ansatz.

1. INTRODUCTION

When Onsager published his solution of the two-dimensional Ising model in 1944,⁽¹⁾ this was almost instantly recognized as a milestone in the development of statistical mechanics. Many new developments were inspired by his results. On the other hand, Onsager's techniques were far ahead of his time and, when he announced his incredibly simple result for the spontaneous magnetization as a comment to a conference talk,^(2,3) his paper

¹Department of Physics, Oklahoma State University, Stillwater, OK 74078-0444, USA.

²Supported in part by NSF Grants Nos. DMS 91-06521 and PHY 93-07816.

attained a mystical status for many years after. That his student Kaufman simplified the solution through Clifford algebras (i.e. fermions)^(4,5) did little to change this.

Now, nearly fifty years later, we can appreciate Onsager’s methods much better. He was the first to introduce the star-triangle equation⁽⁶⁾ to statistical mechanics^(1,3) even though now the name Yang-Baxter equation is commonly used.^(7–10) He also was the first to introduce loop algebras⁽¹¹⁾ as a solvability principle. Onsager and Kaufman have clear priority over Wick for the Wick theorem⁽⁵⁾ and, together with Bethe,⁽¹²⁾ they scouted a new area of mathematics which is now called quantum groups.^(13–17)

Onsager’s (only partly published) work on two-point functions in the Ising model got extended in 1966,^(18–20) but it was only in 1973, when Wu, McCoy, Tracy, and Barouch^(21–23) announced the Painlevé equation for the scaled two-point correlation, that the theory of the two-dimensional Ising model went beyond Onsager’s level. Also, the first two-dimensional models solved that were more complicated than the Ising model were Lieb’s ice model^(24,25) of 1967 and Baxter’s eight-vertex model⁽⁹⁾ of 1973.

Onsager’s loop-algebra solution method was generalized only in 1985 when Von Gehlen and Rittenberg⁽²⁶⁾ solved the Dolan-Grady⁽²⁷⁾ criterium within a one-dimensional generalization of the quantum Potts model. The connection with Onsager’s 1944 paper was noticed by Perk,^(28,29) showing that the chiral Potts model^(30,31,10) is the first genuine generalization of the Ising model, with its “superintegrable” case⁽³²⁾ solvable for two reasons: star-triangle integrability^(30,31,10) and loop-algebra integrability.^(28,26) The chiral Potts model upgrades the fermions of Kaufman⁽⁴⁾ to parafermions.³ It also provides an infinite hierarchy of quantum groups at roots of unity, with Ising as its first entry.^(35,36) Thus the works of Onsager are still at the center of attention.

This paper is organized as follows: In section 2 we define the chiral Potts model and review some of the exact results obtained so far.^(37–41) We pay special attention to the interfacial tensions ϵ_r , giving several results that have not been presented before as such.⁴ We show that the solvable chiral

³We note that the parafermions here are of “cyclic root-of-unity” type,⁽³³⁾ generalizing the Weyl algebra, not of the more usual “highest-weight” type introduced by Green.⁽³⁴⁾ Within the original Ising model and its fermion approaches these two types are isomorphic, however.

⁴We gratefully acknowledge several private communications with Dr. Baxter.

Potts models “superwet,” that is $\epsilon_r = r\epsilon_1$, at $T = 0$ and $T = T_c$. However, Baxter^(38,39) has shown that, for $0 < T < T_c$, the interfacial tensions satisfy the inequalities $\epsilon_r < \epsilon_{r-j} + \epsilon_j$, so that the integrable line is in the not-wetted region. We use low-temperature expansions and the exact results of Baxter to further analyze the effects of various boundary conditions. We also discuss what the critical exponents obtained exactly mean for the scaling function. In sections 3 to 5, we discuss the relation between the integrable subcases, whose Boltzmann weights can be represented by a product-form, and the generalized clock-model representations of the pair-interaction energies. Special attention is given to the symmetric case (with equal horizontal and vertical interactions) and several numerical details and graphs are given. In section 6, we outline a Bethe Ansatz calculation for the leading corrections to the zero-temperature diagonal interfacial tensions. Finally, in section 7, we introduce a new model with only few parameters, which is very close to the integrable model and may deserve detailed further study by numerical means.

2. CHIRAL POTTS MODEL

2.1. Integrable Chiral Potts Model

In our original paper,⁽³⁰⁾ new exact-solution manifolds were discovered within the chiral Potts model. To be more specific, the Potts model,^(42–44) which is itself a generalization of the two-dimensional Ising model solved by Onsager⁽¹⁾ in 1944, and whose interaction energy for the two spins on an edge is given by

$$\mathcal{E}(\sigma, \sigma') = E \delta_{\sigma, \sigma'}, \quad (2.1)$$

was generalized to the chiral Potts model (or \mathbb{Z}_q -model⁽⁴³⁾) with interaction energy

$$\mathcal{E}(\sigma, \sigma') = \mathcal{E}(n - n') = \sum_{j=1}^{N-1} E_j \omega^{j(n-n')}, \quad (2.2)$$

where

$$\omega = e^{2\pi i/N}, \quad \sigma = \omega^n, \quad \sigma' = \omega^{n'}. \quad (2.3)$$

Clearly the interaction energy defined by (2.2) satisfies the relation $\mathcal{E}(\sigma, \sigma') = \mathcal{E}(n - n') = \mathcal{E}(n - n' + N)$. For $E_j = E$, ($1 \leq j \leq N - 1$), using

$$\sum_{j=1}^{N-1} \omega^{j(n-n')} = N\delta_{\sigma, \sigma'} - 1, \quad (2.4)$$

we find that the interaction energy is identical to that of the Potts model except for an overall constant. When $E_j = E_{N-j}$, it includes the integrable Fateev-Zamolodchikov⁽⁴⁵⁾ self-dual \mathbb{Z}_N model as a special case.

The Boltzmann weight for an edge is

$$W(n - n') = e^{-\mathcal{E}(n-n')/k_B T} \quad (2.5)$$

with k_B the Boltzmann constant. Since duality transform is equivalent to Fourier transform^(42,43) of these weights, the weights are said to be “self-dual,” if they are equal (or proportional) to their Fourier transforms. With a great deal of effort^(30,46,47) and some luck we were able to find self-dual solutions to the star-triangle equations and found that they can be written in product forms.

In Australia, Baxter and the two of us^(31,10) — mainly through guessing and especially guided by Onsager’s work⁽¹⁰⁾ — found more general solutions of the star-triangle or “checkerboard Yang-Baxter” equation,

$$\sum_{d=1}^N \overline{W}_{qr}(b-d) W_{pr}(a-d) \overline{W}_{pq}(d-c) = R_{pqr} W_{pq}(a-b) \overline{W}_{pr}(b-c) W_{qr}(a-c). \quad (2.6)$$

They are also given in product form. To be more specific, we found that in the chiral Potts model, the weights W_{pq} or \overline{W}_{pq} depend on two line (or rapidity) variables denoted by $\mathbf{p} \equiv (x_p, y_p, \mu_p)$ and $\mathbf{q} \equiv (x_q, y_q, \mu_q)$, shown in Fig. 1; the weights are given as

$$\frac{W_{pq}(n)}{W_{pq}(n-1)} = \left(\frac{\mu_p}{\mu_q} \right) \left(\frac{y_q - x_p \omega^n}{y_p - x_q \omega^n} \right), \quad \frac{\overline{W}_{pq}(n)}{\overline{W}_{pq}(n-1)} = (\mu_p \mu_q) \left(\frac{\omega x_p - x_q \omega^n}{y_q - y_p \omega^n} \right). \quad (2.7)$$

Here, the parameters \mathbf{p} and \mathbf{q} are restricted by the two periodicity requirements $W_{pq}(N+n) = W_{pq}(n)$ and $\overline{W}_{pq}(N+n) = \overline{W}_{pq}(n)$, yielding the conditions

$$\left(\frac{\mu_p}{\mu_q} \right)^N = \frac{y_p^N - x_q^N}{y_q^N - x_p^N}, \quad (\mu_p \mu_q)^N = \frac{y_q^N - y_p^N}{x_p^N - x_q^N}. \quad (2.8)$$

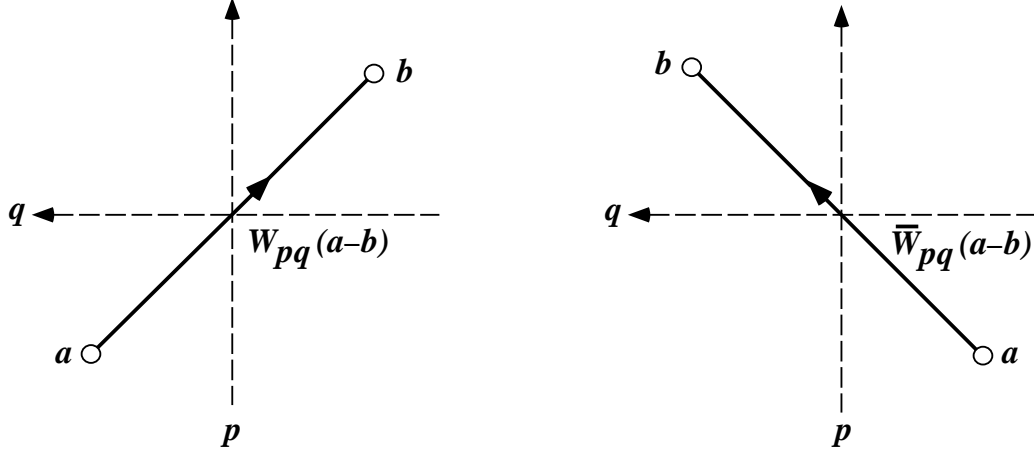


Fig. 1. Boltzmann weights $W_{pq}(a-b)$ and $\bar{W}_{pq}(a-b)$ for two types of edges connecting spins a and b . As $W(a-b) \neq W(b-a)$, and similarly for \bar{W} , we need to put arrows on the edges to distinguish the two different choices.

These imply the existence of numbers k and k' related by $k^2 + k'^2 = 1$ such that the equations

$$\mu_p^N = k'/(1 - kx_p^N) = (1 - ky_p^N)/k', \quad x_p^N + y_p^N = k(1 + x_p^N y_p^N) \quad (2.9)$$

hold for each \mathbf{p} . (This may require using the ambiguity in defining the x_p , x_q , y_p , and y_q in (2.7) and rescaling them with a common factor.) The equations (2.9) describe a complex curve, and the genus of this curve is $g = N^2(N-2) + 1$.

From Fig. 2, one can see that the star-triangle equations allow one to move the rapidity line \mathbf{p} through the vertex (the intersection of the other two rapidity lines). Because of this, one can permute these rapidity lines without changing the partition function, except possibly some constant factors. Baxter called such lattice models Z -invariant.⁽⁴⁸⁾ This also means that transfer matrices associated with different rapidity variables commute. We can see from (2.7) to (2.9) that for given k , there is only one free variable x_p , associated with each rapidity variable \mathbf{p} , and that y_p and μ_p can be determined from (2.9). For the rectangular lattice with just two rapidity variables p and q , and therefore two kinds of weights W_{pq} and \bar{W}_{pq} , there are three free variables.

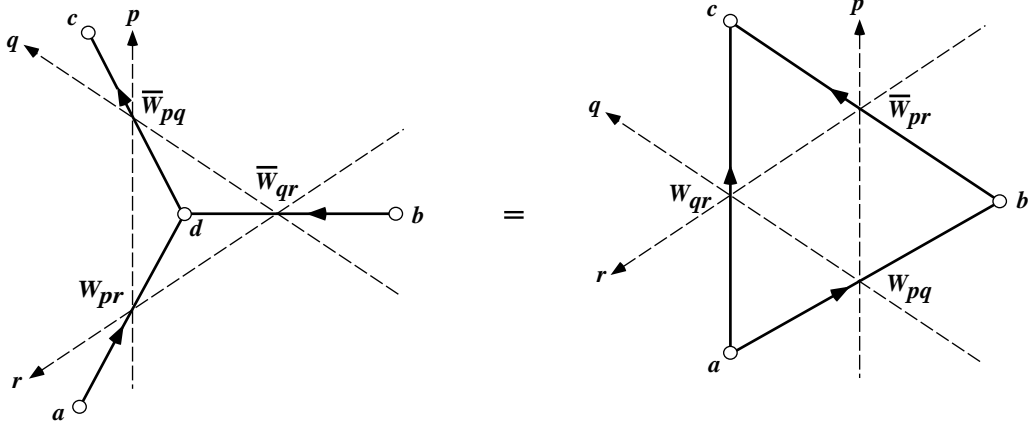


Fig. 2. The star-triangle relations, allowing one to move the rapidity line p through a vertex, which is the intersection of the two other rapidity lines q and r .

By comparing with the Ising model $(N = 2)^{(1)}$ where k and k' are the elliptic modulus and its complementary modulus, we conclude that k and k' describe how far the system is from its critical point.

2.2. Gauge Transformations

Moreover, let

$$\eta_p = \eta(x_p, k), \quad W_{pq}(n)' = \left(\frac{\eta_p}{\eta_q}\right)^n W_{pq}(n), \quad \overline{W}_{pq}(n)' = (\eta_p \eta_q)^n \overline{W}_{pq}(n), \quad (2.10)$$

for any arbitrary function η . We can then replace the W and \overline{W} in (2.6) by the W' and \overline{W}' in (2.10). We find that, if $W_{pq}(n)$ and $\overline{W}_{pq}(n)$ satisfy (2.6), then $W_{pq}(n)'$ and $\overline{W}_{pq}(n)'$ also satisfy the star-triangle equations (2.6).

Furthermore, the transformation (2.10) leaves the partition function for a system with periodic boundary conditions invariant. This can be seen easily by examining what happens at a particular site e under such a transformation in a checkerboard lattice with p , p' , q , and q' as the rapidity variables, as shown in Fig. 3. One finds that the additional factor η_q^e in $\overline{W}_{pq}(e-d)'$ cancels out the factor η_q^{-e} in $W_{p'q}(e-c)'$, and the η_p^e in $\overline{W}_{pq}(e-d)'$ cancels out the η_p^{-e} in $W_{pq'}(a-e)'$, etc, leaving the net contribution at each site unchanged.

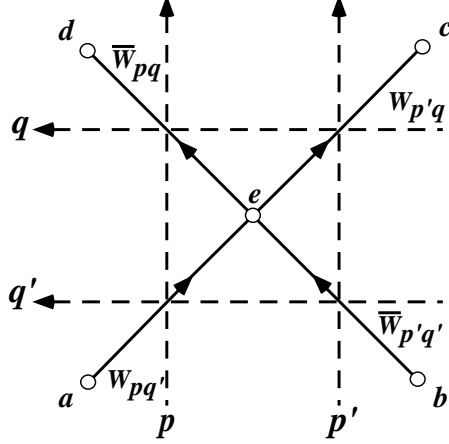


Fig. 3. Gauge transformation at a particular site e adds gauge factors to each of the four Boltzmann weights associated with the four bonds meeting in e . The total contributions add up to zero.

Particularly, if we choose $\eta_p = \mu_p^{-1}$, then $W_{pq}(n)'$ and $\overline{W}_{pq}(n)'$ are no longer periodic, and they differ from (2.7) by dropping the μ_p and μ_q factors, making the weights and transfer matrices depend rationally on x_p , x_q , y_p , and y_q only, and therefore more manageable. Indeed, as we are left only with the last equation in (2.9) the genus of the curve is then reduced to $g = (N - 1)^2$.

On the other hand, if $\eta(x, k)$ in (2.10) is a constant function, then only \overline{W} picks up a factor. When we let $\eta_p = \eta_q = \omega^\rho$, then \overline{W} remains periodic, whenever ρ is an integer.

2.3. Integrable Model and Zero-Temperature Limit

We now compare the weights of the integrable model with the weights given by (2.5) and (2.2), which has $2(N - 1)$ variables E_j and \overline{E}_j . Hence for (2.2) to be integrable, there must be $2N - 5$ equations between these $2N - 2$ variables. We rewrite the $2(N - 1)$ variables as

$$\begin{aligned} -\frac{E_j}{k_B T} &= K_j \omega^{\Delta_j}, & -\frac{E_{N-j}}{k_B T} &= K_j \omega^{-\Delta_j}, \\ -\frac{\overline{E}_j}{k_B T} &= \overline{K}_j \omega^{\overline{\Delta}_j}, & -\frac{\overline{E}_{N-j}}{k_B T} &= \overline{K}_j \omega^{-\overline{\Delta}_j}, \end{aligned} \quad (2.11)$$

for $1 \leq j \leq [N/2]$, with $[x]$ denoting the integral part of x . Therefore (2.2) becomes

$$-\frac{\mathcal{E}(n)}{k_B T} = \begin{cases} \sum_{j=1}^{\frac{1}{2}(N-1)} 2K_j \cos\left(\frac{2\pi}{N}(jn + \Delta_j)\right), & N \text{ odd}, \\ \sum_{j=1}^{\frac{1}{2}N-1} 2K_j \cos\left(\frac{2\pi}{N}(jn + \Delta_j)\right) + K_{\frac{1}{2}N}(-1)^n, & N \text{ even}, \end{cases} \quad (2.12)$$

with similar equations for $\bar{\mathcal{E}}$. For real K_j and Δ_j , the Boltzmann weights are real and positive. When N is odd, we can think of the interactions as composed of $\frac{1}{2}(N-1)$ chiral clock model terms; particularly, for $N=3$, it is the three-state chiral clock model. For even N there is an additional Ising-like term; for example, for $N=4$, it is composed of a four-state clock model with an Ising term.

The weights of the integrable models given in (2.7) through (2.9) can be rewritten in the form

$$\frac{W(n)}{W(0)} = \frac{((1, \alpha))_{0,n}}{((1, \beta))_{0,n}}, \quad \frac{\bar{W}(n)}{\bar{W}(0)} = \frac{((1, \bar{\alpha}))_{0,n}}{((1, \bar{\beta}))_{0,n}}, \quad (2.13)$$

where we have used the definitions

$$((1, \alpha))_{m,n} = \frac{(1, \alpha)_{m,n}}{\Delta(\alpha)^{n-m}}, \quad \Delta(\alpha) = (1 - \alpha^N)^{1/N}, \quad (1, \alpha)_{m,n} = \prod_{j=m+1}^n (1 - \omega^j \alpha), \quad (2.14)$$

for $m < n$. It is easy to verify that

$$((1, \alpha))_{m,n} = ((1, \alpha))_{m,k} ((1, \alpha))_{k,n}. \quad (2.15)$$

Since $((1, \alpha))_{m,m} = 1$, we can extend the definition to $m > n$ by

$$((1, \alpha))_{m,n} = 1/((1, \alpha))_{n,m}. \quad (2.16)$$

Moreover, because of the normalization factor $\Delta(\alpha)$, we have

$$((1, \alpha))_{m,m+N} = 1. \quad (2.17)$$

Hence, the weights in (2.13) are always periodic with period N .

In order that the weights (2.13) satisfy the star-triangle equations (2.6), they have to satisfy only one necessary condition on the four constants α , β , $\bar{\alpha}$, and $\bar{\beta}$, namely

$$\frac{\alpha}{\beta} = \frac{\bar{\beta}}{\omega \bar{\alpha}}. \quad (2.18)$$

This is consistent with (2.7); it can also be derived directly. Substituting $W(n)$, $\bar{W}(n)$ (for W_{pq} and \bar{W}_{pq}), $W'(n)$, and $\bar{W}'(n)$ (for W_{pr} and \bar{W}_{pr}), as given by (2.13), into (2.6), we can solve $W''(n)$, and $\bar{W}''(n)$ (for W_{qr} and \bar{W}_{qr}), provided

$$\frac{\alpha}{\bar{\beta}} = \frac{\beta}{\omega \bar{\alpha}} = \frac{\alpha'}{\bar{\beta}'} = \frac{\beta'}{\omega \bar{\alpha}'}, \quad \frac{\Delta(\alpha)\Delta(\bar{\alpha})}{\Delta(\beta)\Delta(\bar{\beta})} = \frac{\Delta(\alpha')\Delta(\bar{\alpha}')}{\Delta(\beta')\Delta(\bar{\beta}')}. \quad (2.19)$$

From this, we precisely reproduce the Z -invariant periodic solutions (2.7) to (2.9), up to possible gauge transformations as mentioned in (2.10). Other than that, the only other allowed variation on the weights is that ω may be chosen to be any root of unity $\omega^N = 1$ or $\omega = e^{2\pi i j/N}$ for any integer $1 \leq j \leq N-1$. Here j and N must be relative prime, otherwise we would need to redefine $\Delta(\alpha)$ in order to retain periodicity. Letting

$$\alpha = e^{2i\theta}, \quad \beta = e^{2i\phi}, \quad \bar{\alpha} = e^{2i\bar{\theta}}, \quad \bar{\beta} = e^{2i\bar{\phi}}, \quad (2.20)$$

then the weights can be rewritten as

$$\begin{aligned} \frac{W(n)}{W(0)} &= \left[\frac{\sin(N\phi)}{\sin(N\theta)} \right]^{n/N} \prod_{j=1}^n \left[\frac{\sin(\theta + \pi j/N)}{\sin(\phi + \pi j/N)} \right], \\ \frac{\bar{W}(n)}{\bar{W}(0)} &= \left[\frac{\sin(N\bar{\phi})}{\sin(N\bar{\theta})} \right]^{n/N} \prod_{j=1}^n \left[\frac{\sin(\bar{\theta} + \pi j/N)}{\sin(\bar{\phi} + \pi j/N)} \right], \end{aligned} \quad (2.21)$$

which are real as long as θ , ϕ , $\bar{\theta}$, and $\bar{\phi}$ are real. Now (2.18) becomes

$$\bar{\phi} - \bar{\theta} = \frac{\pi}{N} - \phi + \theta. \quad (2.22)$$

Therefore, the weights are functions of three independent variables. We can relate the “elliptic modulus” k with these three variables as most of the exact results are given in terms of this k . Comparing (2.7) with (2.13), we find

$$\alpha = e^{2i\theta} = \frac{x_p}{y_q}, \quad \beta = e^{2i\phi} = \frac{x_q}{y_p}, \quad \bar{\alpha} = e^{2i\bar{\theta}} = \frac{x_q}{\omega x_p}, \quad \bar{\beta} = e^{2i\bar{\phi}} = \frac{y_p}{y_q}. \quad (2.23)$$

Therefore

$$e^{2i(\theta-\phi)} = \frac{x_p y_p}{x_q y_q}, \quad e^{2i(\phi-\bar{\theta})} = \frac{\omega x_p}{y_p}, \quad e^{2i(\theta+\bar{\theta})} = \frac{x_q}{\omega y_q}. \quad (2.24)$$

We can then use (2.9) to obtain

$$k^2 = \sin^{-2} \left(N(\theta - \phi) \right) \left[\cos^2 \left(N(\theta + \bar{\theta}) \right) + \cos^2 \left(N(\phi - \bar{\theta}) \right) - 2 \cos \left(N(\theta + \bar{\theta}) \right) \cos \left(N(\phi - \bar{\theta}) \right) \cos \left(N(\theta - \phi) \right) \right]. \quad (2.25)$$

This is also easily verified substituting (2.24) in the right-hand side of (2.25) and eliminating y_p^N and y_q^N using the last equality in (2.9).

In section 3, we express θ and ϕ in (2.20) and (2.21) in terms of the $N-1$ variables K_j and Δ_j of (2.12). Clearly, these variables must satisfy $N-3$ consistency relations. The four variables θ , ϕ and $\bar{\theta}$, $\bar{\phi}$ can be easily rewritten in terms of K_j , Δ_j , \bar{K}_j , $\bar{\Delta}_j$. The integrability condition (2.22) gives another condition relating them.

For the square lattice with $\bar{W} = W$, (which is called the symmetric case in the following), it then follows from (2.21) that we must have $\bar{\theta} = \theta$ and $\bar{\phi} = \phi$. Consequently, the integrability condition becomes

$$\phi - \theta = \frac{\pi}{2N} \quad \text{or} \quad \phi = \theta + \frac{\pi}{2N}. \quad (2.26)$$

Now it is very easy to express $K_j = \bar{K}_j$ and $\Delta_j = \bar{\Delta}_j$ in terms of the single variable θ , and plot graphs for different N . The details are included in section 5 and here we outline a few of the conclusions. We find, with the energy unit convention $k_B T K_1 = 1$ of subsection 5.2, that the integrable curve ends at zero temperature at

$$\begin{aligned} -\mathcal{E}(n) &= \sum_{j=1}^{N-1} \frac{\sin(\pi/N)}{\sin(\pi j/N)} \cos \left(\frac{2\pi n j}{N} \pm \left(\frac{1}{2} - \frac{j}{N} \right) \pi \right) \\ &= \sum_{l=1}^{N-1} \frac{\sin(\pi/N)}{\sin(\pi l/N)} \omega^{ln \mp (2l-N)/4} \\ &= \left(N \pm 2n - 1 + 2N[\mp \frac{n}{N}] \right) \sin \frac{\pi}{N}. \end{aligned} \quad (2.27)$$

The last form is linear in n , periodically extended, with $[x]$ again denoting the integral part of x . The first form in (2.27) hides the linearity with n , but

will suggest an interesting generalization. As the temperature T increases, Δ_1 decreases, and on the integrable line, the ratios K_j/K_1 and Δ_j/Δ_1 remain almost constant for $1 \leq j \leq [\frac{1}{2}(N-1)]$, namely

$$\frac{K_j}{K_1} = \frac{\sin(\pi/N)}{\sin(\pi j/N)} + \kappa_j, \quad \frac{\Delta_j}{\Delta_1} = \frac{N-2j}{N-2} + \delta_j, \quad (2.28)$$

with $\kappa_j, \delta_j \lesssim 0.02$. For $\Delta_j = 0$, the self-dual and therefore critical case, we have

$$K_{jc} = \sum_{m=1}^N \frac{\sin(\pi j(2m-1)/N)}{2N \sin(\pi j/N)} \log \left[\frac{\sin((m - \frac{1}{4})\pi/N)}{\sin((m - \frac{3}{4})\pi/N)} \right]. \quad (2.29)$$

The curves of $1/K_j$ versus Δ_k are symmetric with respect to the vertical axis.

2.4. Boundary Conditions and Interfacial Tension at $T=0$

In the study of the interfacial tensions in model systems,^(37–39,49–55) various boundary conditions and different orders of taking the limit are being used. We shall here examine the resulting differences, using the chiral clock model as an example.

In almost all of the numerical studies of the chiral clock model, fixed boundary conditions are preferred. Specifically, in the work of Yeomans and Derrida,⁽⁵³⁾ they consider a lattice with \mathcal{L} rows and \mathcal{M} columns, as shown in Fig. 4, and demand that the spins on the boundary rows have fixed values: $\sigma(m, 0) = r$ and $\sigma(m, \mathcal{L}) = 0$; but they impose periodic (or cyclic) boundary conditions on the utmost left and right columns. They choose to have finite \mathcal{L} , but $\mathcal{M} \rightarrow \infty$; that is, in the direction along the interface, the system is infinite from the start.

Huse et al., in their low-temperature analysis⁽⁴⁹⁾ of the wetting transition for the symmetric case with $W = \overline{W}$, consider a lattice oriented diagonally with L rows and M columns,⁵ as shown in Fig. 5. The spins in the top row have fixed values r and in the bottom row they are 0. Moreover, they find it convenient to pin the diagonal interface in the middle by further demanding the spins in the upper halves of the boundary columns to have the fixed values

⁵We have made a trivial reflection. They have a “vertical” interface, whereas we have a “horizontal” one.

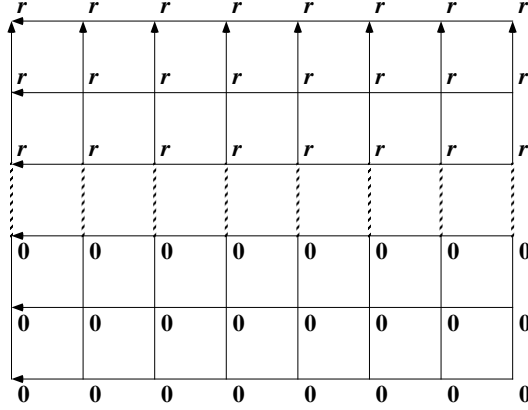


Fig. 4. Interface at zero temperature in a lattice with \mathcal{L} rows and \mathcal{M} columns. The interaction between a vertical nearest-neighbor pair of spins, ω^n and $\omega^{n'}$, is $\mathcal{E}(n - n')$, while it is $\overline{\mathcal{E}}(n - n')$ for a horizontal pair.

r , and in the lower halves fixed values 0. That is $\sigma(0, \ell) = \sigma(M, \ell) = r$ for $0 \leq \ell \leq \frac{1}{2}L$ and $\sigma(0, \ell) = \sigma(M, \ell) = 0$ for $\frac{1}{2}L < \ell \leq L$. Their analysis is done by taking $L \rightarrow \infty$ first, then $M \rightarrow \infty$; that is, in the direction perpendicular to the interface, the system is infinite from the start.

In the analytical works of Baxter,^(37–39) such a diagonally oriented lattice is being used for computational convenience, because the diagonal transfer matrices form commuting families. Just as in the Ising model, where Onsager obtained the interfacial tension⁽¹⁾ by imposing antiperiodic and periodic ($N = 2$) boundary conditions, here skew boundary conditions are imposed on the top and bottom boundary “rows,” that is $\sigma_{m, L+1} = \sigma_{m, 0} - r$, ($r = 0, \dots, N-1$), for the two boundary spins in the same “column,” while cyclic boundary conditions are imposed on the two utmost left and right boundary columns with $\sigma(0, \ell) = \sigma(M, \ell)$. Due to such skew boundary conditions, a “horizontal” (actually, diagonal) interface occurs. The skew boundary conditions do not affect the commutation properties.⁽¹⁰⁾

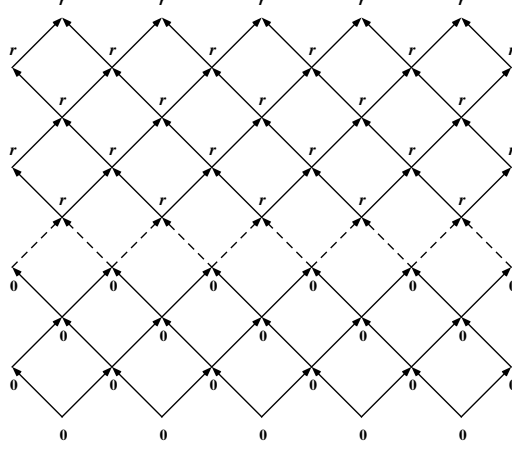


Fig. 5. Interface at zero temperature for the symmetric case with $W = \overline{W}$ in a lattice with M diagonal columns and L diagonal rows, with skew boundary conditions imposed on top and bottom rows and periodic boundary conditions on the utmost left and right columns.

2.4.1. Interfacial Tension at $T=0$

At zero temperature only ground states contribute to the partition function Z , and to its logarithm, which is proportional to the free energy F . We would typically expect a low-temperature behavior

$$-\log Z \equiv \frac{F}{k_B T} = \frac{E_g}{k_B T} - \Sigma_0 + o(T), \quad (2.30)$$

where E_g is the ground-state energy, Σ_0 is an entropic term related to the ground-state degeneracy, and $o(T)$ stands for (usually exponentially) small corrections. In this subsection, we shall concentrate on the ground-state energy and surface or interface corrections to the bulk behavior of it.

In the ferromagnetic case, $\mathcal{E}(r) < \mathcal{E}(0)$, $\overline{\mathcal{E}}(r) < \overline{\mathcal{E}}(0)$ for $r \neq 0$, and with the fixed boundary conditions mentioned above, the ground state has to have a seam or interface. For the lattice shown in Fig. 4, the excess free energy at $T = 0$, or the increase in the ground-state energy due to the mismatch of spins in two adjacent rows, divided by the interface length \mathcal{M} , is defined to be the horizontal interfacial tension ϵ_r . Hence the interfacial tensions at

$T = 0$ are given by⁶

$$\epsilon_r = \delta\mathcal{E}(-r) \equiv \mathcal{E}(-r) - \mathcal{E}(0) > 0, \quad \text{for } r = 1, \dots, N-1. \quad (2.31)$$

Now, from (2.27), we find that the $N-1$ interfacial tensions of the symmetric integrable chiral Potts model at $T = 0$ satisfy

$$\epsilon_r = 2r \sin \frac{\pi}{N} = r\epsilon_1 = \epsilon_{r-1} + \epsilon_1, \quad (2.32)$$

which is a consequence of the special form of the W weights.

Hence, at zero temperature, this not only signifies a wetting transition, but for $N > 3$ a more special phenomenon is taking place which we shall call “superwetting,” with the maximal amount of interface degeneracy as each interface of type r is free to break up into two interfaces of types j and $r-j$, for any j between 1 and $r-1$.⁷ It is as if we have energy levels given by spin operators S^z for $2S+1 = N$, similar to what happens in the superintegrable chiral Potts model.^(26,32)

It should be obvious that the horizontal couplings $\bar{\mathcal{E}}$ have no role to play at zero temperature. Particularly, for the three-state chiral clock model, there is no difference in the horizontal interfacial tension between the symmetric case with $\mathcal{E}(n) = \bar{\mathcal{E}}(n)$ and the Ostlund-Huse asymmetric case with the same $\Delta_1 \neq 0$ but $\bar{\Delta}_1 = 0$.

On the other hand, if we interchange $\mathcal{E}(n)$ and $\bar{\mathcal{E}}(n)$, then the incremental free energy due to the mismatch is now, for the Ostlund-Huse $N = 3$ case,

$$\delta\bar{\mathcal{E}}(-1) = \delta\bar{\mathcal{E}}(1) = 3, \quad \delta\bar{\mathcal{E}}(r) \equiv \bar{\mathcal{E}}(r) - \bar{\mathcal{E}}(0), \quad (2.33)$$

different from

$$\delta\mathcal{E}(\mp 1) = 3 \cos\left(\frac{2\pi}{3}\Delta_1\right) \mp \sqrt{3} \sin\left(\frac{2\pi}{3}\Delta_1\right) = 2\sqrt{3} \sin\left(\frac{\pi}{3}(1 \mp 2\Delta_1)\right). \quad (2.34)$$

⁶Several statements in this subsection also apply to nonzero temperatures, provided we replace excess energies by excess free energies per “surface area” (length) \mathcal{A} . The resulting interfacial tensions or surface tensions are independent of the choice of the ensemble and its corresponding thermodynamic potential, as long as, with the “surface volume” (area) V^s , each surface order parameter or its corresponding surface field vanishes.⁽⁵⁶⁾

⁷Interfacial wetting can occur only in systems with three or more bulk phases ($N > 2$), contrary to surface wetting which can occur in the Ising model ($N \geq 2$).⁽⁵⁷⁾ However, “surface superwetting” also requires $N > 2$ and interfacial superwetting $N > 3$.

Thus the excess in free energies at $T = 0$ calculated for the asymmetric case are different in the two directions. This means that the interfacial tensions are anisotropic. We denote the angle-dependence by letting $\epsilon_r = \epsilon_r(\varphi)$, whenever confusion may occur, with $\epsilon_r(0)$ denoting the horizontal, $\epsilon_r(\frac{1}{2}\pi)$ the vertical, and $\epsilon_r(\frac{1}{4}\pi)$ the diagonal interfacial tension.

The diagonal interfacial tension at zero temperature can also be calculated by considering the incremental ground-state energy due to the mismatch of bonds in a lattice, for example as shown by dashed lines in Fig. 5. Following Baxter,^(38,39) we calculate the incremental energy per horizontal and vertical bond pair. For the symmetric case with $W = \overline{W}$, we find

$$\epsilon_r = 2\delta\mathcal{E}(-r) = 4r \sin(\pi/N), \quad (2.35)$$

which is double the amount in (2.32) and the same whether cyclic or free boundary conditions are imposed on the left and right boundary columns. Again this shows that the integrable model is at a superwetting transition at zero temperature.

For the asymmetric cases, however, the diagonal interfacial tensions at $T = 0$ are given by

$$\epsilon_r(\frac{1}{4}\pi) = \delta\mathcal{E}(-r) + \delta\overline{\mathcal{E}}(-r). \quad (2.36)$$

For the three-state Ostlund-Huse model at $\Delta_1 = \frac{1}{4}$, we have

$$\delta\mathcal{E}(-1) = \sqrt{3}, \quad \delta\mathcal{E}(-2) = 2\sqrt{3}, \quad \delta\overline{\mathcal{E}}(-1) = \delta\overline{\mathcal{E}}(-2) = 3. \quad (2.37)$$

Substituting these into (2.36), we find that $\frac{1}{2}\epsilon_1(\frac{1}{4}\pi)$ is greater than $\epsilon_1(0)$ given in (2.32) and $\frac{1}{2}\epsilon_2(\frac{1}{4}\pi)$ is smaller than $\epsilon_2(\frac{1}{2}\pi)$ in (2.32). Hence this diagonal interfacial tension, as well as the vertical interfacial tensions, in the Ostlund-Huse asymmetric case with $W \neq \overline{W}$, do not satisfy the superwetting condition even at $T = 0$.

At zero temperature, we can also easily find the interfacial tensions for general angle $0 \leq \varphi \leq \frac{1}{2}\pi$, as

$$\epsilon_r(\varphi) = \mathcal{N}(\varphi)^{-1} \left(\delta\mathcal{E}(-r) \cos \varphi + \delta\overline{\mathcal{E}}(-r) \sin \varphi \right), \quad (2.38)$$

which can be normalized⁸ per horizontal (or vertical) bond using

$$\mathcal{N}(\varphi) = \max(\cos(\varphi), \sin(\varphi)). \quad (2.39)$$

⁸For the excess energy per unit length we would have to use $\mathcal{N}(\varphi) = 1$.

Such a ground state is highly degenerate as there are many configurations of the interface with a given number of horizontal and vertical bonds. For ground-state wetting we need that either a horizontal or a vertical piece of the interface wets. So, for $N = 3$ the system is not wet when both $0 \leq \Delta_1, \overline{\Delta}_1 < \frac{1}{4}$, and it is wet when at least one of the $\Delta_1, \overline{\Delta}_1 \geq \frac{1}{4}$ within the interval $0 \leq \Delta_1, \overline{\Delta}_1 \leq \frac{1}{2}$. A ground-state wetting transition occurs for

$$\Delta_1 = \frac{1}{4}, \quad 0 \leq \overline{\Delta}_1 \leq \frac{1}{4} \quad \text{or} \quad 0 \leq \Delta_1 \leq \frac{1}{4}, \quad \overline{\Delta}_1 = \frac{1}{4}, \quad (2.40)$$

which is the boundary of these two regimes.

At $\Delta_1 = \frac{1}{2}$, we find from (2.33) and (2.34) that

$$\delta\mathcal{E}(-1) = 0, \quad \delta\mathcal{E}(-2) = 3, \quad \delta\overline{\mathcal{E}}(-1) = \delta\overline{\mathcal{E}}(-2) = 3. \quad (2.41)$$

Now we can use (2.36) to find that the diagonal interfacial tensions do satisfy the condition for the onset of wetting: $\epsilon_2 = 2\epsilon_1$. This means that the wetting transition of the diagonal interface of the Ostlund-Huse model occurs at $T = 0$ and $\Delta_1 = \frac{1}{2}$. It is interesting to note that the chiral melting line starts at the same point. The finite-strip calculations of Yeomans and Derrida⁽⁵³⁾ show that even the vertical interface (which is parallel to the chiral field) is wet at this point. It is interesting to investigate whether the wetting curve of the diagonal interface is identical to the chiral melting curve.

We shall now consider some other subtleties of the interfacial tensions, as they relate to different boundary conditions and different orders of taking the thermodynamic limit. We shall restrict ourselves to diagonally oriented lattices only.

2.4.2. The Limit $M \rightarrow \infty$, then $L \rightarrow \infty$

If one lets the number of columns $M \rightarrow \infty$ first and the number of rows $L \rightarrow \infty$ afterwards, then the boundary condition imposed on the columns should not have any effect. This can also be seen by considering the elements of the column transfer matrix $T^{(0r)}$ with finite L — dividing by the largest eigenvalue of $T^{(00)}$ (the bulk term). At non-zero temperature, these elements are all positive and thus the Perron-Frobenius theorem holds. Consequently, the largest eigenvalue is nondegenerate. In the limit $M \rightarrow \infty$, only the largest eigenvalue survives. This shows that the resulting interfacial tension is independent of the boundary conditions imposed on the columns for $T > 0$.

Nevertheless, in this limit, the interfacial tensions depend heavily on the boundary conditions imposed on the top and bottom rows. We may consider the interface (or domain wall) as a random walker,⁽⁵²⁾ who tends to walk in the direction of higher probability. For the skewed boundary condition, this allows an interface winding around the cylinder of length L and perimeter M crossing the seam of modified bonds several times. Thus for the Ostlund-Huse model, with⁽⁴⁹⁾

$$\begin{aligned}x \equiv w_1 &\equiv W(-1)/W(0), \quad y \equiv w_2 \equiv W(-2)/W(0), \\z \equiv \overline{w}_1 &\equiv \overline{W}(-1)/\overline{W}(0) = \overline{w}_2 \equiv \overline{W}(-2)/\overline{W}(0), \\x &< z < y,\end{aligned}\tag{2.42}$$

the ϵ_1 interface prefers to walk perpendicular to the chiral field and then continue by crossing the seam, while the ϵ_2 interface tends to walk parallel to the chiral field, as shown in Figs. 6a and 6b. Thus one does obtain the horizontal interfacial tension $\epsilon_1(0)$ and the vertical interfacial tension $\epsilon_2(\frac{1}{2}\pi)$ using a diagonally oriented lattice with skewed boundary conditions. For fixed boundary conditions on the boundary rows, one obtains instead the diagonal interfacial tensions $\epsilon_r(\frac{1}{4}\pi)$. Specifically, we find

$$\begin{aligned}\text{skewed b.c.:} \quad & \lim_{L \rightarrow \infty} \lim_{M \rightarrow \infty} k_B T \log(Z_r/Z_0) = \min_{\theta} \epsilon_r(\theta), \\ \text{fixed b.c.:} \quad & \lim_{L \rightarrow \infty} \lim_{M \rightarrow \infty} k_B T \log(Z_{0r}/Z_{00}) = \epsilon_r(\tfrac{1}{4}\pi),\end{aligned}\tag{2.43}$$

where Z_r and Z_{0r} denote the corresponding partition functions.

In the latter case, with fixed boundary conditions for the boundary spins, we have free open boundary conditions for the domain walls, which can touch but not cross the boundaries. On the other hand, a seam due to skewed boundary conditions can be moved to any place using gauge transformations. In spite of the Perron-Frobenius theorem, these two cases are very different, even in the limit $M \rightarrow \infty$, when the size of the row transfer matrix becomes infinite.

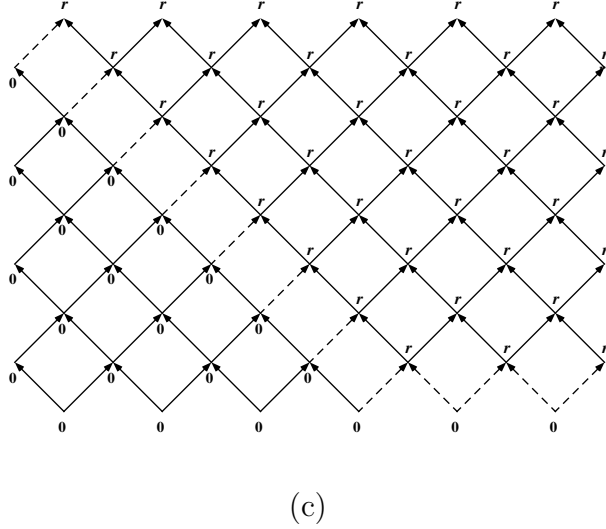
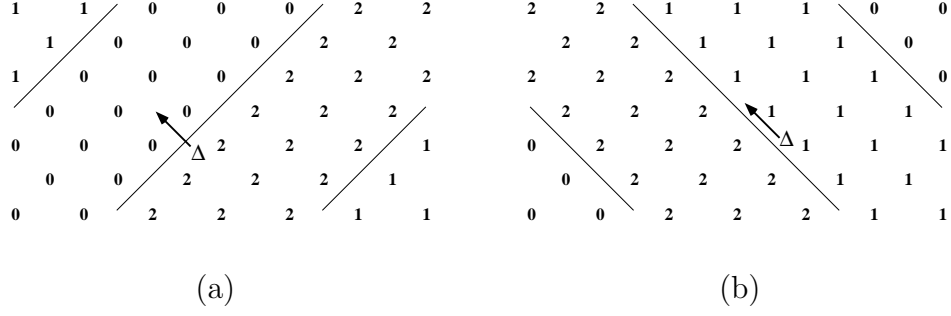


Fig. 6. (a) For the case with skewed boundary conditions in both directions, an interface is allowed to wind around the torus of vertical perimeter L and horizontal perimeter M , crossing the seams of modified bonds several times. Thus for the Ostlund-Huse model, a single-step interface with tension ϵ_1 prefers to walk perpendicular to the chiral field and then continue by crossing the seams. (b) A double-step interface with tension ϵ_2 tends to walk parallel to the chiral field. (c) If fixed boundary conditions are imposed on the top and bottom rows, and free boundary conditions imposed on the outer columns, it is energetically more favorable for the system to arrange itself into a configuration with a mismatch. Therefore if we let $M \rightarrow \infty$, and fix the ratio $M/L > 1$, the excess in free energy at $T = 0$ can have any arbitrary value depending on M/L .

2.4.3. The Limit $L \rightarrow \infty$, then $M \rightarrow \infty$

If we take the limit that the number of rows $L \rightarrow \infty$ first, then it is necessary to pin the interface roughly at the middle⁹ in order to get a true ϵ_r interface. Otherwise, because there are L positions to place the ϵ_r interface, while there are $\binom{L}{r}$ possible positions to place the r ϵ_1 interfaces, the term with r ϵ_1 interfaces dominates the partition function, in this limit.

Now it is easy to see that the boundary conditions on the top and bottom rows can have no impact, as an interface of finite length M could not possibly reach the boundary rows which are infinitely far away. On the other hand, with one end of the interface being pinned to the middle, cyclic boundary conditions imposed on the boundary columns force the interface to come back giving the diagonal interfacial tension, while free boundary conditions on the boundary columns allow the interface to wander and settle to its lowest energy configuration, yielding the minimum of the interfacial tensions.

2.4.4. The Limit $L, M \rightarrow \infty$, with fixed M/L

In exact calculations, however, it is cumbersome to pin the interface in the middle. As Baxter⁽³⁹⁾ chooses to let $M, L \rightarrow \infty$ simultaneously, we shall examine the case when they are proportional to one another. Since the Perron-Frobenius theorem may not hold on infinite matrices, a difference in boundary conditions could play an important role.

The full complexity seems to arise when $M/L > 1$. It is most interesting to consider the case when fixed boundary conditions are imposed on the top and bottom rows and free boundary conditions on the columns. Then it is easily seen that it is energetically more favorable for the system to arrange itself into a configuration with a mismatch as shown in Fig. 6c. Therefore, if we let $M \rightarrow \infty$ and fix the ratio $M/L > 1$, the excess in free energy at $T = 0$ can have any arbitrary value depending on M/L . A similar problem arises, when skewed boundary conditions are imposed on the top and bottom rows. For if the ratio M/L is an integer, or free boundary conditions are imposed on the boundary columns, we will obtain the minimum of the two interfacial tensions shown in Figs. 6a and 6b; otherwise, the interfacial tension will be a function of M/L .

⁹This is equivalent to the subtraction procedure used by Baxter⁽³⁸⁾ who needs to omit an $L^2 Z_1^2$ term from Z_2 in order to obtain ϵ_2 , see his (5.27), (A9), and surrounding text.

For $M/L < 1$, however, this complexity disappears, and cyclic boundary conditions on the columns give the diagonal interfacial tensions, whereas free boundary conditions give the minimum of the interfacial tensions over all directions. Thus by taking the limits in an appropriate way, we may calculate horizontal or vertical interfacial tensions using a diagonally oriented lattice.

2.4.5. Single Interface at Low Temperatures

Let us now discuss the effect of boundary conditions on the restricted partition functions with one domain wall. As before, M denotes the size of the system in the direction of the interface, and L the size perpendicular to it. Besides the partition function without the domain wall $Z_0(L, M)$, we can introduce various partition functions with a single domain wall. First, we can introduce $Z_{1,\text{pin}}(L, M|s)$ for the partition function with the interface pinned in the middle on one side and pinned s steps from the middle on the other side. We can also introduce $Z_{1,\text{per}}(L, M)$ for the periodic case, where the interface starts and ends at the same, but otherwise free, position, and $Z_{1,\text{free}}(L, M)$ for the case where the interface is left free on both sides. These three partition functions are closely related when L becomes large, namely

$$\begin{aligned}\frac{Z_{1,\text{per}}(L, M)}{Z_0(L, M)} &\approx L \lim_{L' \rightarrow \infty} \frac{Z_{1,\text{pin}}(L', M|0)}{Z_0(L', M)}, \\ \frac{Z_{1,\text{free}}(L, M)}{Z_0(L, M)} &\approx L \sum_{s=-\infty}^{+\infty} \lim_{L' \rightarrow \infty} \frac{Z_{1,\text{pin}}(L', M|s)}{Z_0(L', M)}.\end{aligned}\quad (2.44)$$

Therefore, these quantities are easily evaluated at low temperatures, for which overhangs can be ignored, using e.g. random walks, transfer matrix techniques, or Szegő's theorems for Toeplitz matrices.

For the horizontal interface as in Fig. 4 and using (2.42), we find

$$\lim_{\mathcal{M} \rightarrow \infty} \lim_{\mathcal{L} \rightarrow \infty} \frac{1}{\mathcal{M}} \log \frac{Z_{1,\text{free}}(\mathcal{L}, \mathcal{M})}{\mathcal{L} Z_0(\mathcal{L}, \mathcal{M})} \approx \log \frac{(1 - xy) \bar{x}}{(1 - x)(1 - y)} \quad (2.45)$$

and

$$\begin{aligned}
& \lim_{\mathcal{M} \rightarrow \infty} \lim_{\mathcal{L} \rightarrow \infty} \frac{1}{\mathcal{M}} \log \frac{Z_{1,\text{per}}(\mathcal{L}, \mathcal{M})}{\mathcal{L} Z_0(\mathcal{L}, \mathcal{M})} \\
& \approx \lim_{\mathcal{L} \rightarrow \infty} \lim_{\mathcal{M} \rightarrow \infty} \frac{1}{\mathcal{M}} \log \frac{Z_{1,\text{fix}}(\mathcal{L}, \mathcal{M})}{Z_{0,\text{fix}}(\mathcal{L}, \mathcal{M})} \approx \log \frac{(1 - xy) \bar{x}}{(1 - \sqrt{xy})^2}, \quad (2.46)
\end{aligned}$$

where “fix” stands for various boundary conditions which keep the interface continuing within a horizontal strip of width \mathcal{L} . The results differ only by exponentially small terms in the temperature T , following a leading term of order $1/T$, showing that “kinks” are important.

However, for the diagonal interface as in Fig. 5, we find

$$\lim_{M \rightarrow \infty} \lim_{L \rightarrow \infty} \frac{1}{M} \log \frac{Z_{1,\text{free}}(L, M)}{L Z_0(L, M)} \approx 2 \log(x + \bar{x}) \quad (2.47)$$

and

$$\begin{aligned}
& \lim_{M \rightarrow \infty} \lim_{L \rightarrow \infty} \frac{1}{M} \log \frac{Z_{1,\text{per}}(L, M)}{L Z_0(L, M)} \\
& \approx \lim_{L \rightarrow \infty} \lim_{M \rightarrow \infty} \frac{1}{M} \log \frac{Z_{1,\text{fix}}(L, M)}{Z_{0,\text{fix}}(L, M)} \approx 2 \log(2\sqrt{x\bar{x}}), \quad (2.48)
\end{aligned}$$

where the factor 2 is to have agreement with Baxter’s convention. Now the differences occur in the order 1, and the corrections are entropic in nature.

From the results (2.45) to (2.48), we see that the effects of the boundary disappear when the system is reflection symmetric with respect to an axis perpendicular to the interface, so that $x = y$ in (2.45) and (2.46), or $x = \bar{x}$ in (2.47) and (2.48). In those two cases, for which the interface is perpendicular to the chiral direction, we can use ref. 49 to obtain further detail.

2.5. Wetting Transitions

Wetting transitions can occur when there are different types of domains and domain walls. More precisely, the wetting transition is defined as “the bubbles of B domain absorbed on the $A\|C$ interface merge into an essentially macroscopic layer of B domain which wets the entire interface,” (see e.g. page 377 of ref. 49). We need to compare a configuration with a domain wall $A\|C$ with a configuration with two domain walls $A|B$ and $B|C$. Hence, the wetting temperature T_w is defined by

$$T_w = \min_{\theta} T_w(\theta), \text{ with } T_w(\theta) \text{ from } \epsilon_2(\theta, T) = 2 \epsilon_1(\theta, T). \quad (2.49)$$

As the interfaces can be oriented differently, the wetting transition can occur at different temperatures $T_w(\theta)$, but its minimum is the true wetting temperature for given chirality Δ_1 .

We note that we need to compare the interfacial tensions $\epsilon_2(\theta)$ and $2\epsilon_1(\theta)$ for the same angle θ , as is implicit in all the calculations mentioned above.^(49–55) It is often energetically more favorable to wet than to turn the interface through an angle for which it is necessary to flip macroscopically many spins. We should be careful not to calculate T_w from $\min \epsilon_2(\theta, T) = 2 \min \epsilon_1(\theta, T)$, as a calculation with skewed boundary conditions in both directions could lead to and which would cause us to overestimate $\Delta_{\text{wet}}(T)$.

It seems that an interface perpendicular to the “chiral field” Δ_1 wets first. In fact, Huse et al. calculate the wetting curve by considering diagonal interfaces for the symmetric case, with $\Delta_{\text{ver}} = \Delta_{\text{hor}}$, and horizontal interfaces for the Ostlund-Huse model with $\Delta_{\text{ver}} \neq 0$ and $\Delta_{\text{hor}} = 0$. Particularly, for the diagonal interface of the Ostlund-Huse model, its wetting line would have to start at zero temperature at $\Delta_1 = \frac{1}{2}$, above the wetting curve of the horizontal interface, which wets at $\Delta_1 = \frac{1}{4}$ and $T = 0$. We note that a diagonal interface is a superposition of many allowed walks with a given number of horizontal and vertical bonds. So with a chiral field in the vertical direction, horizontal segments of the interface will wet at $\frac{1}{4}$, while vertical segments will not wet, lowering $\Delta_{\text{wet}}(T=0)$ from $\frac{1}{2}$ to $\frac{1}{4}$.

It is easy to extend the low-temperature analysis of Huse et al.⁽⁴⁹⁾ to the case with $K_1 \neq \overline{K}_1$ and one finds that, at low temperature, the wetting line for the Ostlund-Huse model, ($\overline{x} = \overline{y} \equiv \overline{z}$), is given by¹⁰

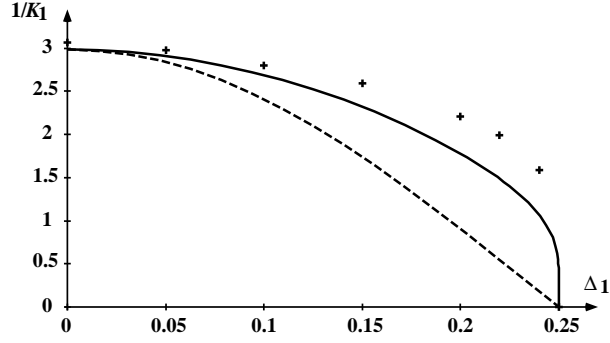
$$\frac{y}{x^2} = \exp \left[6K_1 \sin \left(\frac{1}{6} \pi (1 - 4\Delta_1) \right) \right] = 1 + 2\overline{z}^2 + O(\overline{z}^3), \quad \overline{z} = \exp(-6\overline{K}_1), \quad (2.50)$$

while the integrable line is given by

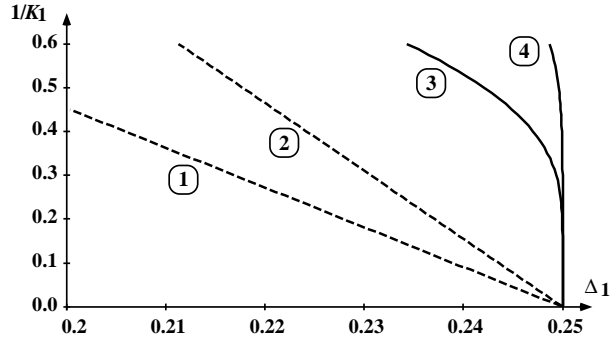
$$\frac{y}{x^2} = 1 + 2\overline{z} + O(\overline{z}^2). \quad (2.51)$$

The integrable line, denoted by line 3, and the wetting line, denoted by line 4, are shown in Fig. 7b. They rise faster than any power due to the importance of kinks, see also the text below (2.46).

¹⁰There is a small discrepancy with a factor 3 given by Huse et al.⁽⁴⁹⁾ instead of 2 as given below, which we believe to be due to a misprint.



(a)



(b)

Fig. 7. (a) Integrable lines in the 3-state chiral clock model. The solid curve is for the Ostlund-Huse fully asymmetric case and the dashed line is for the symmetric case. The crosses are the numerical results of Stella et al. for the fully asymmetric case. (b) We enlarge the part of the graph for T small and Δ_1 near $\frac{1}{4}$, with the integrable lines marked as lines 1 and 3. We have also plotted the results of Huse et al. with line 2 denoting the wetting line of the symmetric lattice, and line 4 the one for the fully asymmetric case. The graphs show that the integrable lines are near but below the wetting lines, with the largest relative deviations in the low-temperature regime.

For the symmetric lattice with $W = \overline{W}$, ($\overline{x} = x, \overline{y} = y$), however, we find that the diagonal interface wets first, with the wetting line given by Huse et al. as

$$\frac{y}{x^2} = \frac{3}{2} + \dots, \quad (2.52)$$

whereas the integrable line is given by

$$\frac{y}{x^2} = 2 + \dots. \quad (2.53)$$

These are also plotted in Fig. 7b as lines 2 and 1 respectively. The wetting curve for the horizontal or vertical interface in the symmetric case also starts at $\Delta_1 = \frac{1}{4}$ and $T = 0$, but rises in a much steeper way. Since all the interfaces wet on this curve, it would be interesting to compare the behaviors near this curve and near the chiral melting curve of the Ostlund-Huse model.

We show in Fig. 7a the integrable line for the 3-state chiral clock^(49–55) model. The solid curve is for the Ostlund-Huse asymmetric case, while the dashed line is for the symmetric case, with equal horizontal and vertical interactions. We can see that both curves end up at the same point for zero temperature. The numerical results of Stella et al.⁽⁵⁵⁾ for the wetting line in the Ostlund-Huse model are represented here by crosses.

In Fig. 7b, we enlarge the graphs for T small and Δ_1 near $\frac{1}{4}$, with the integrable lines marked as lines 1 and 3 added to the wetting line results of Huse et al. with line 2 for the symmetric lattice and line 4 for the fully asymmetric case. The curves show that the integrable lines are near but below the wetting lines. For $0 < T < T_c$, therefore, contrary to what we have conjectured before,⁽¹⁰⁾ and in agreement with Baxter,^(38,39) we find that the integrable model is in the non-wetted region.

2.6. Low-Temperature Regimes

As suggested to us by Baxter,¹¹ we can approximate the Boltzmann weights of the integrable chiral Potts model,

$$w_n \equiv \frac{W(-n)}{W(0)} = \frac{1}{\Lambda^n} \prod_{j=0}^{n-1} \left[\frac{\sin(j\lambda - \phi)}{\sin(j\lambda - \theta)} \right],$$

¹¹Private communications.

$$\overline{w}_n \equiv \frac{\overline{W}(-n)}{\overline{W}(0)} = \frac{1}{\overline{\Lambda}^n} \prod_{j=0}^{n-1} \left[\frac{\sin(j\lambda - \overline{\phi})}{\sin(j\lambda - \overline{\theta})} \right], \quad (2.54)$$

where

$$\lambda \equiv \frac{\pi}{N} = \phi + \overline{\phi} - \theta - \overline{\theta}, \quad \Lambda^N \equiv \frac{\sin(N\phi)}{\sin(N\theta)}, \quad \overline{\Lambda}^N \equiv \frac{\sin(N\overline{\phi})}{\sin(N\overline{\theta})}, \quad (2.55)$$

see also (2.7), (2.21), and section 4, by replacing $\theta, \overline{\theta}, \phi, \overline{\phi}$ inside the products in (2.54) by their zero-temperature limiting values. For the symmetric case, with

$$-\lambda < \theta \equiv \overline{\theta} < -\frac{3}{4}\lambda, \quad \phi \equiv \overline{\phi} = \theta + \frac{1}{2}\lambda, \quad (2.56)$$

we can express θ and ϕ in terms of k using (2.25). We find successively

$$\begin{aligned} k &= \cos(2N\theta), \quad \sin(N\theta) = -\sqrt{\frac{1}{2}(1-k)}, \quad \sin(N\phi) = -\sqrt{\frac{1}{2}(1+k)}, \\ \Lambda^N &= \overline{\Lambda}^N = \sqrt{\frac{1+k}{1-k}} = \frac{1+k}{k'}, \quad \phi = \overline{\phi} = -\frac{1}{N} \arcsin \sqrt{\frac{1}{2}(1+k)}, \\ \theta = \overline{\theta} &= -\frac{1}{N} \left(\pi - \arcsin \sqrt{\frac{1}{2}(1-k)} \right) = \phi - \frac{\pi}{2N}. \end{aligned} \quad (2.57)$$

The zero-temperature limit then corresponds to

$$\theta \equiv \overline{\theta} \rightarrow -\lambda, \quad \phi \equiv \overline{\phi} \rightarrow -\frac{1}{2}\lambda, \quad \Lambda \equiv \overline{\Lambda} \equiv \left(\frac{1+k}{k'} \right)^{1/N} \rightarrow \infty, \quad (2.58)$$

and we find the asymptotic low-temperature formula for the weights

$$w_n = \overline{w}_n = \frac{1}{\Lambda^n} \prod_{j=1}^n \frac{\sin\left((j - \frac{1}{2})\lambda\right)}{\sin(j\lambda)}. \quad (2.59)$$

Here we can allow $\overline{\Lambda} \neq \Lambda$, as this corresponds to a gauge transformation.

Baxter applied a Bethe Ansatz method with skew-periodic boundary conditions,⁽³⁸⁾ shown in Fig. 5, together with a complicated subtraction method, in order to obtain the first two diagonal interfacial tensions in the low-temperature regime. Indeed, substituting

$$f = g = \tan^2(\tfrac{1}{2}\lambda), \quad \chi_0 = 0, \quad (2.60)$$

corresponding to the symmetric case, his results (5.36) and (A12) reduce to

$$\begin{aligned}\frac{\epsilon_1}{k_B T} &= -\log(4w_1\bar{w}_1) = 2\log\left(\Lambda \cos(\tfrac{1}{2}\lambda)\right), \\ \frac{\epsilon_2}{k_B T} - 2\frac{\epsilon_1}{k_B T} &= \log\left((1-f^2)^2\right) = 2\log\left(1 - \tan^4(\tfrac{1}{2}\lambda)\right),\end{aligned}\quad (2.61)$$

or, equivalently,

$$\begin{aligned}\frac{\epsilon_1}{k_B T} &= 2\log \Lambda + \log\left(1 + \tan^2(\tfrac{1}{2}\lambda)\right), \\ \frac{\epsilon_2}{k_B T} &= 4\log \Lambda + 2\log\left(1 - \tan^2(\tfrac{1}{2}\lambda)\right).\end{aligned}\quad (2.62)$$

These results are useful to verify that the exact calculations⁽³⁹⁾ based on analytic continuation from the superintegrable case are correct.

For the symmetric case, there is an easier Bethe Ansatz calculation than the one done by Baxter,⁽³⁸⁾ namely one with free boundary conditions. This gives the desired results directly, without a subtraction procedure. As we do not only have to consider “collisions” of interfaces, but also reflections at the boundary, we use an extension of the Bethe Ansatz⁽¹²⁾ similar to the ones introduced by Gaudin.⁽⁵⁸⁾ But as this requires further consistency conditions, our method does not apply to asymmetric cases that differ from (2.59) by more than changing Λ to $\bar{\Lambda}$ for \bar{w} . We shall outline our Bethe Ansatz calculations in section 6. These calculations show some special features on the integrable line, which may be related to some pre-wetting phenomena.

We note that the Bethe Ansatz method to calculate interfacial tensions in the low-temperature limit is similar to the Müller-Hartmann–Zittartz approximation⁽⁵¹⁾ in ignoring overhangs. Moreover, that method can be also used for non-symmetric and non-integrable cases, with the condition

$$y/x^2 = e^{6K_1 \sin(\pi(1-4\Delta_1)/6)}, \quad \bar{y}/\bar{x}^2 = e^{6\bar{K}_1 \sin(\pi(1-4\bar{\Delta}_1)/6)} \quad \text{finite.} \quad (2.63)$$

However, for more than two interfaces the additional condition $y/x^2 = \bar{y}/\bar{x}^2$ is needed for the Bethe Ansatz to work.

The above procedure (2.58) to obtain the low-temperature expansion also works for asymmetric cases with

$$\theta, \bar{\theta} \rightarrow -\lambda, \quad k \rightarrow 1, \quad \bar{\phi} = -\lambda - \phi, \quad \text{with } \phi \not\rightarrow -\lambda \text{ or } 0. \quad (2.64)$$

Later on in section 4 we shall see that this represents just one part of the integrable manifold in the phase diagram for the 3-state chiral clock

model. So we shall call models with (2.64) “quasi-symmetric” cases. It is a regime which does not include, nor even border, fully asymmetric cases as the Ostlund-Huse model, for which the vertical weights satisfy the condition $\overline{W}(n) = \overline{W}(-n)$ while the horizontal weights are chiral, $W(n) \neq W(-n)$.

As we shall show for $N = 3$ later in section 4, to have $\overline{W}(n) = \overline{W}(-n)$, we must require

$$\overline{\theta} = -\lambda - \overline{\phi}, \quad \text{with} \quad \overline{\Lambda} = 1. \quad (2.65)$$

Together with the integrability condition (2.55), we find then that there can be only two free variables, say θ and ϕ , such that

$$\overline{\theta} = -\lambda - \frac{1}{2}(\theta - \phi), \quad \overline{\phi} = \frac{1}{2}(\theta - \phi), \quad (2.66)$$

Because of that, in the low-temperature limit given by $\theta, \overline{\theta} \rightarrow -\lambda$, we must also have $\phi \rightarrow -\lambda$. In order to see whether the integrable model is or is not in the wetted region, it is necessary to include higher order terms in the low-temperature expansion. In fact, for the three-state Ostlund-Huse model, the condition $K = \overline{K}$ reduces the free variables to just one, and in the low-temperature limit, $\phi \rightarrow -\frac{1}{3}\pi + \delta\phi$, we find $\theta = -\frac{1}{3}\pi + \delta\phi^\rho$ with $\rho = (1 + \sqrt{3})$. (The details are delegated to section 4). Therefore, we have

$$\frac{w_2}{w_1^2} = \frac{y}{x^2} = O(\delta\phi) \sim \overline{w}_1 = \overline{w}_2 = z = \frac{\sin[\frac{1}{2}(\phi - \theta)]}{\sin[\frac{1}{3}\pi - \frac{1}{2}(\phi - \theta)]}. \quad (2.67)$$

Because these are of the same order of magnitude, we have to take kinks in the interface into account,⁽⁴⁹⁾ as also noted below (2.46).

It seems that the largest asymmetric integrable regime is described by $\overline{\phi} \rightarrow 0$, $\theta, \overline{\theta}, \phi \rightarrow \lambda$. For $N = 3$, this corresponds to $\overline{K} = K$ and $\overline{\Delta} = p\Delta$, ($p \neq 0, 1$), which again reduces the parameters to just one. We find

$$\phi = -\frac{1}{3}\pi + \delta\phi, \quad \theta = -\frac{1}{3}\pi + \delta\theta, \quad \overline{\phi} = -\delta\overline{\phi}, \quad \overline{\theta} = -\frac{1}{3}\pi + \delta\overline{\theta}, \quad (2.68)$$

with

$$\delta\theta \approx \delta\phi \left(\frac{2}{\sqrt{3}} \delta\phi \right)^{\sqrt{b^2+b+1}}, \quad \delta\overline{\phi} \approx \delta\phi, \quad \delta\overline{\theta} \approx \delta\phi \left(\frac{2}{\sqrt{3}} \delta\phi \right)^{b-1}, \quad (2.69)$$

where

$$b = \sin\left(\frac{1}{6}(1+p)\pi\right) / \sin\left(\frac{1}{6}(1-p)\pi\right). \quad (2.70)$$

For limits as in (2.64), we shall show in section 4 that

$$\Delta_1 = \frac{1}{4} - \frac{\kappa}{K_1} + \dots, \quad \overline{\Delta}_1 = \frac{1}{4} - \frac{\overline{\kappa}}{\overline{K}_1} + \dots, \quad (2.71)$$

with κ and $\overline{\kappa}$ some positive constants. This shows that both Δ and $\overline{\Delta} \rightarrow \frac{1}{4}$ as $T \rightarrow 0$, which is rather restricted.

2.7. Baxter's Exact Interfacial Tension Results, Symmetric Case

In two recent papers,^(38,39) Baxter obtained several new exact results for the interfacial tensions in the integrable chiral Potts model. At this moment, it is not clear to us if or how we can extract from his results the interfacial tensions for the fully asymmetric Ostlund-Huse case. Here we shall work out his results in explicit detail only for the fully symmetric case, leaving the results for the more general case implicit for now.

In equation (42) of Baxter's second paper, we can substitute⁽³⁹⁾

$$\begin{aligned} u_q = v_q = \frac{\pi}{2N} = \frac{1}{2}\lambda, \quad \Lambda_q = \sqrt{\frac{1+k}{1-k}}, \quad \eta_p = 1, \quad \eta_q = \eta, \\ \eta^{N/2} = \frac{\Lambda_q - 1}{\Lambda_q + 1} = \sqrt{\frac{1-k'}{1+k'}}, \quad k' \equiv \sqrt{1-k^2}, \quad m = m_0 = 1, \end{aligned} \quad (2.72)$$

resulting in the very explicit formula for the interfacial tensions

$$\frac{\epsilon_r}{k_B T} = 2v_r(m_0) = \frac{8}{\pi} \int_0^\eta dy \frac{\sin(\frac{\pi r}{N})}{1 + 2y \cos(\frac{\pi r}{N}) + y^2} \operatorname{artanh} \sqrt{\frac{\eta^N - y^N}{1 - \eta^N y^N}}, \quad (2.73)$$

in the symmetric case. Here η is a temperature-like variable on the integrable curve, defined in (2.72).

In the low-temperature region,

$$k' \approx \frac{1}{2}N(1 - \eta) \rightarrow 0, \quad (2.74)$$

we can expand (2.73) as

$$\frac{\epsilon_r}{k_B T} = -\frac{2r}{N} \log(\frac{1}{2}k') - \overline{\sigma}_{r,N} + O(k'), \quad (2.75)$$

where the constant is given by a dilogarithm integral, which seems different from the ones studied recently by Kirillov and many others,^(59,60)

$$\begin{aligned}\bar{\sigma}_{r,N} &\equiv \frac{4}{\pi} \int_0^1 dx \frac{\sin(\frac{\pi r}{N})}{1 + 2x \cos(\frac{\pi r}{N}) + x^2} \log\left(\frac{1+x^N}{1-x^N}\right) \\ &= \log\left(\frac{1}{\cos^2(\frac{1}{2}r\lambda)} \prod_{j=1}^{[\frac{1}{2}r]} \frac{\cos^4\left(\frac{1}{2}(r-2j+1)\lambda\right)}{\cos^4\left(\frac{1}{2}(r-2j)\lambda\right)}\right).\end{aligned}\quad (2.76)$$

This also satisfies the sum rule

$$\sum_{j=1}^{N-1} \bar{\sigma}_{j,N} = \log N. \quad (2.77)$$

We have not found a direct way yet to prove the last equality in (2.76), except for the cases $N = 2$ (Ising) and $N = 3$. In section 6, we shall outline an indirect proof using a Bethe Ansatz method. We originally guessed the formula by performing numerical integration to 100 places and expanding the exponentials of the integrals in periodic continued fractions, which gave us

$$\bar{\sigma}_{1,2} = \log 2, \quad \bar{\sigma}_{1,3} = \log \frac{4}{3}, \quad \bar{\sigma}_{2,3} = \log \frac{9}{4}, \quad (2.78)$$

$$\begin{aligned}\bar{\sigma}_{1,4} &= \log(2(2 - \sqrt{2})), \quad \bar{\sigma}_{2,4} = -\log(2(2 - \sqrt{2})^2), \\ \bar{\sigma}_{3,4} &= \log(4(2 - \sqrt{2})),\end{aligned}\quad (2.79)$$

$$\begin{aligned}\bar{\sigma}_{1,5} &= \log(2(5 - \sqrt{5})/5), \quad \bar{\sigma}_{2,5} = \log(5/4), \\ \bar{\sigma}_{3,5} &= \log(32/(5 - \sqrt{5})^3), \quad \bar{\sigma}_{4,5} = \log(5(5 - \sqrt{5})^2/16).\end{aligned}\quad (2.80)$$

Combining these results with Baxter's two Bethe Ansatz results⁽³⁸⁾ for $r = 1$ and 2, see also (2.62) in the previous subsection, we originally guessed (2.76).

For the critical region,

$$\eta^{\frac{1}{2}N} \approx \frac{1}{2}k \rightarrow 0, \quad (2.81)$$

we can expand (2.73) by first expanding the artanh in a Taylor series of its argument. Then, it is straightforward to rewrite the integrand in (2.73) as a

power series of y and η , multiplied with $\sqrt{\eta^N - y^N}$. Each term of the series leads to a Beta function integral, $B(x, y) = \Gamma(x)\Gamma(y)/\Gamma(x + y)$. We find

$$\frac{\epsilon_r}{k_B T} = \frac{8 \sin(\frac{\pi r}{N}) B(\frac{1}{N}, \frac{1}{2})}{\pi(N + 2)} \eta^{\frac{1}{2}N+1} - \frac{8 \sin(\frac{2\pi r}{N}) B(\frac{2}{N}, \frac{1}{2})}{\pi(N + 4)} \eta^{\frac{1}{2}N+2} + O(\eta^{\frac{1}{2}N+3}), \quad (2.82)$$

giving both the leading term⁽³⁹⁾ and the first correction term. Coefficients of further terms $\eta^{\frac{1}{2}N+j}$, for $j = 3, 4, \dots$, can also be obtained easily.

2.8. Other Exact Results and Further Speculations

A great deal of progress on the chiral Potts models has been achieved. The exponent α for the specific heat — not to be confused with the independent variables for the integrable weights given in (2.13) — has been obtained by Baxter⁽⁴⁰⁾ for the case with real positive Boltzmann weights and the exponents β_j of the one-point functions $\langle \sigma^j \rangle$ have been conjectured by Albertini et al.⁽³²⁾ They are

$$\alpha = 1 - \frac{2}{N}, \quad \beta_j = \frac{j(N - j)}{2N^2}. \quad (2.83)$$

In fact, Albertini et al.⁽³²⁾ also conjectured the exact low-temperature formula

$$\langle \sigma^j \rangle = (1 - k'^2)^{\beta_j} = k^{2\beta_j}, \quad (2.84)$$

which generalizes the Onsager result^(2,3) for the spontaneous magnetization of the Ising model.

For $N = 3$, we find $\alpha = \frac{1}{3}$, which is identical to the three-state Potts model result. It is generally believed that the chiral field Δ_1 is a relevant variable, and the free energy in the scaling region can be written as

$$F(T, \Delta_1, \overline{\Delta}_1, H) = F(T, \Delta_1, p\Delta_1, H) = |t|^{2-\alpha} X(g\Delta_1/|t|^\phi, hH/|t|^\psi), \quad (2.85)$$

for some crossover exponents ϕ and ψ and with $t = T/T_c - 1$, where T_c is the Potts critical point. The ratio of the two chiral fields $\overline{\Delta}_1/\Delta_1$ is believed to be an irrelevant variable, which may only change the two constants g and h .

The exact calculation of Baxter⁽⁴⁰⁾ gives

$$F(T, \Delta_1, \overline{\Delta}_1, 0) \sim |k^2|^{2-\alpha}, \quad (2.86)$$

where k is the elliptic modulus given by (2.23), with $k = 0$ for $T = T_c$ and $\Delta_1 = \overline{\Delta}_1 = 0$.

For $k \sim 0$, we find the integrable line lies on the curve given by

$$t = -9.959616982 (1 + p^2) \Delta_1^2 + O(t^2, t \Delta_1^2, \Delta_1^4), \quad p = \overline{\Delta}_1 / \Delta_1, \quad (2.87)$$

and

$$k^2 \sim \frac{108 (2 + \sqrt{3}) K_{1c}^2}{1 + K_{1c} (7\sqrt{3} + 12)} t = -4.981050242 t, \quad (2.88)$$

with $K_{1c} = J_1 / k_B T_c = \frac{1}{3} \log(1 + \sqrt{3})$, see also eq. (4.26). In the above equation, $p = 1$ corresponds to the symmetric case and $p = 0$ to the Ostlund-Huse asymmetric case. The analytic expansion (2.87) for the integrable line is similar in form to the usual expression for the nonlinear thermal scaling field⁽⁴⁹⁾

$$\tilde{t} = t + c_2 \Delta_1^2 + \dots, \quad (2.89)$$

in terms of which the free energy can be rewritten as

$$F(T, \Delta_1, \overline{\Delta}_1, H) = |\tilde{t}|^{2-\alpha} X(g \Delta_1 / |\tilde{t}|^\phi, h H / |\tilde{t}|^\psi). \quad (2.90)$$

But to say more about this requires more detail from exact results than we currently have available.

From the most recent results in (2.82), we conclude that we have the following asymptotic expansions for the surface tensions on the integrable line,

$$\epsilon_r = |t|^{\frac{1}{2} + \frac{1}{N}} D_r(|t|^{\frac{1}{N}}), \quad (2.91)$$

which we must compare with the forms required by scaling

$$\epsilon_r = |t|^\mu D_r(\Delta_1 / |t|^\phi). \quad (2.92)$$

Now, as the temperature is an analytic function of Δ_1 on the integrable line, we need

$$\Delta_1 \sim |t|^{\frac{1}{2}}, \quad (2.93)$$

and we find

$$\mu = \frac{1}{2} + \frac{1}{N}, \quad \phi = \frac{1}{2} - \frac{1}{N}. \quad (2.94)$$

The critical exponents are most conveniently expressed in terms of the scaling (conformal) dimensions x_j and y_j , indicating how a local density (or

order parameter) m_j and its corresponding field scale with a typical length scale R in the problem,

$$m_j \sim R^{-x_j}, \quad h_j \sim R^{-y_j}, \quad x_j + y_j = 2. \quad (2.95)$$

In our model, the subscript j takes the values T (thermal), $1, \dots, N-1, \Delta$ (chiral), with $h_T \equiv t \equiv (T - T_c)/T_c$, $m_j \equiv \langle \sigma^j \rangle$ for $j = 1, \dots, N-1$, and $h_\Delta \equiv \Delta_1$.

In terms of these, the usual critical exponents are

$$\begin{aligned} \nu = \mu = \frac{1}{y_T}, \quad \eta_j = 2x_j, \quad 2 - \alpha = \frac{2}{y_T}, \quad \psi_j = \frac{x_j}{y_T} \\ \beta_j = \frac{x_j}{y_T}, \quad \gamma_{ij} = \frac{y_i - x_j}{y_T} = \frac{2 - x_i - x_j}{y_T}, \quad \delta_j = \frac{y_j}{x_j}, \end{aligned} \quad (2.96)$$

where we use ψ_j for the gap exponents (or crossover exponents), as the more conventional notation Δ would lead to confusion. We are writing $\phi \equiv \psi_\Delta$ for the chiral crossover exponent in (2.85).

This leads to the scaling dimensions

$$\begin{aligned} x_T = \frac{4}{N+2}, \quad x_j = \frac{j(N-j)}{N(N+2)}, \quad x_\Delta = \frac{N+6}{N+2}, \\ y_T = \frac{2N}{N+2}, \quad y_j = 2 - x_j, \quad y_\Delta = \frac{N-2}{N+2} = y_T - 1. \end{aligned} \quad (2.97)$$

For $N = 3$, we find $\phi = \frac{1}{6}$, $x_\Delta = \frac{9}{5}$, in agreement with earlier predictions.^(61,55) For general N , $y_\Delta = y_T - 1$ provides the chiral exponents of the Fateev-Zamolodchikov model.⁽⁴⁵⁾

The most detailed results have been obtained for the superintegrable model with weights given by

$$\frac{W(n)}{W(0)} = \frac{((1, \alpha))_{0,n}}{((1, \beta))_{0,n}}, \quad \frac{\overline{W}(n)}{\overline{W}(0)} = \frac{((1, \beta/\omega))_{0,n}}{((1, \alpha))_{0,n}}. \quad (2.98)$$

For the corresponding hermitian quantum spin chain, Albertini et al.⁽⁴¹⁾ have calculated results for the excitation spectrum, demonstrating the special role of level crossings, as the Perron-Frobenius theorem does not apply to this case. Baxter⁽³⁷⁾ has calculated the bulk and surface free energies, horizontal

and vertical interfacial tensions and finite size corrections for the lattice shown in Fig. 6 with free or fixed spin configurations on the left and right columns. He has found that the critical exponents for these physical quantities are given by

$$\begin{aligned}\alpha &= 1 - \frac{2}{N}, & \alpha_s &= 2 - \frac{2}{N}, \\ \mu_{\text{hor}} = \nu_{\text{hor}} &= \frac{2}{N}, & \mu_{\text{ver}} = \nu_{\text{ver}} &= 1, \\ \nu_{\text{hor}} + \nu_{\text{ver}} &= 2 - \alpha.\end{aligned}\tag{2.99}$$

These are extremely interesting and puzzling results, deserving a great deal of attention. Even though the weights are asymmetric, one should not associate ν_{ver} to be in the direction of the vertical weight, because the lattice is oriented diagonally. The two different correlation lengths are obtained from the decay of the finite size effects of such diagonally oriented lattices. Since the diagonal lattice is symmetric under 90° rotation, one is forced to conclude the different boundary conditions give rise to the two different exponents for correlation lengths.

Yet it is remarkable that the bulk properties should be influenced by the boundary, particularly as the partition functions in the superintegrable case are real. In the most recent work of Baxter,^(38,39) he imposes cyclic and skew boundary conditions on the two directions, finding that $2\mu = 2 - \alpha = 1 + 2/N$. Assuming $\mu = \nu$, then the usual scaling relation again holds and, with such boundary conditions, we would have that the vertical and horizontal correlation lengths have the same exponents with $\nu_{\text{ver}} = \nu_{\text{hor}} = 1/2 + 1/N$.

In the superintegrable case, the weights are complex. By a gauge transform, we can make the weights real, but we cannot make them all positive. Therefore the Perron-Frobenius theorem does not hold. This may be the only plausible reason for the above strange behavior. Because the bulk properties can be shown to be boundary dependent for non-positive weights — complex weights are typical within the integrable chiral Potts model — the combination of using Z -invariance properties and analytic continuation, as used by Baxter, may or may not lead to valid results for the positive-real Boltzmann weight case. For this reason, we find it necessary to verify some of the calculations of Baxter by low-temperature expansions.

For real and positive weights, such boundary-dependent behavior is not conceivable. Furthermore, because the anisotropy $p = \overline{\Delta}_1/\Delta_1$ is an irrelevant variable, the exponent ν cannot be a function of p either, therefore we must

have $\nu_{\text{hor}} = \nu_{\text{ver}} = \nu_{\text{dia}} = \nu$. Baxter^(38,39) found that $\mu_{\text{dia}} = 1/2 + 1/N$. Hence, assuming the scaling relation $\mu = \nu$, one finds that the scaling relation $2\nu = 2 - \alpha = 1 + 2/N$ again holds.

2.9. A New Model

In 5.2 we shall present plots, for $N = 7$, of $1/K_2$ and $1/K_3$ versus $1/K_1$, and of Δ_2 and Δ_3 versus Δ_1 . The curves look like straight lines. Plots for $N = 5, 6$ also give the same impression. Yet an explicit calculation shows that the ratios K_j/K_1 and Δ_j/Δ_1 are almost but not quite constant. We therefore propose a new model with constant ratios, given by

$$-\frac{\mathcal{E}(n)}{k_B T} = K \sum_{j=1}^{N-1} \frac{\sin(\pi/N)}{\sin(\pi j/N)} \cos\left(\frac{2\pi}{N}(nj + (N-2j)\Delta)\right), \quad (2.100)$$

which has only two parameters. This may be good for further numerical studies. For $\Delta = \frac{1}{4}$ and $K = -E/k_B T$, (2.100) and (2.27) are identical. Hence at zero temperature, it goes through a superwetting transition at $\Delta = \frac{1}{4}$. In section 7, we shall describe some of the symmetries of this model and show that for $\Delta = \frac{1}{4}(N+1)/(N-1)$ we have $\mathcal{E}(0) = \mathcal{E}(-1)$. Hence, its ground state is highly degenerate, as it is in the chiral clock model;^(50,54) thus this model, like the chiral clock model, can also be used to describe commensurate-incommensurate transitions.

For $T > 0$, we shall show that for a certain value of Δ , this model is not very different from the integrable chiral Potts model. We can use the universality hypothesis to argue that this model in two dimensions, having the same \mathbb{Z}_N symmetry as the integrable chiral Potts model, must have the same exponents. Hopefully, the exact results obtained for the chiral Potts model can be used to gauge the accuracy of the numerical studies.

3. CONSISTENCY EQUATIONS AND INVERSE PROBLEM

In this section we derive the consistency equations that the weights must satisfy in order to be put in product forms as in (2.13). We also express the variables α and β in terms of these weights.

3.1. Consistency Conditions for General N

Let us introduce the notation

$$f(n) = \frac{W(n)W(N-1)}{W(n-1)W(0)}. \quad (3.1)$$

Then substituting (2.13) and (2.14) into it, we find that the $\Delta(x)$ terms cancel out leaving

$$f(n) = \frac{(1 - \alpha\omega^n)(1 - \beta)}{(1 - \beta\omega^n)(1 - \alpha)}, \quad 1 \leq n \leq N-1. \quad (3.2)$$

Now we use (2.20) to rewrite

$$\begin{aligned} \cot(\pi n/N) &= -i \frac{1 + \omega^n}{1 - \omega^n}, \\ \cot \theta &= -i \frac{1 + \alpha}{1 - \alpha}, \quad \cot \phi = -i \frac{1 + \beta}{1 - \beta}. \end{aligned} \quad (3.3)$$

Consequently, (3.2) become $N-1$ linear equations for $\cot \theta$ and $\cot \phi$, i.e.

$$\cot \theta - f(n) \cot \phi = (f(n) - 1) \cot(\pi n/N), \quad 1 \leq n \leq N-1. \quad (3.4)$$

The determinant of any three of these equations must vanish in order to have nontrivial solutions. This gives the consistency equations

$$\sin\left(\frac{(n-2)\pi}{N}\right) (f(n)-1)(f(2)-f(1)) = \sin\left(\frac{n\pi}{N}\right) (f(1)-1)(f(n)-f(2)), \quad (3.5)$$

for $3 \leq n \leq N-1$. Thus if the weights $W(n)$ and $\overline{W}(n)$ satisfy these $N-3$ consistency equations, then they can be put in the product form.

We note that (3.5) is equivalent to the more general equation

$$\frac{(f(n_1) - f(n_2))(f(n_3) - f(n_4))}{(f(n_1) - f(n_4))(f(n_2) - f(n_3))} = \frac{\sin\left(\frac{\pi}{N}(n_1 - n_2)\right) \sin\left(\frac{\pi}{N}(n_3 - n_4)\right)}{\sin\left(\frac{\pi}{N}(n_1 - n_4)\right) \sin\left(\frac{\pi}{N}(n_2 - n_3)\right)} \quad (3.6)$$

which is solved by any expression of the form

$$f(n) \rightarrow \frac{x_1\omega^n + x_2}{x_3\omega^n + x_4}. \quad (3.7)$$

One can solve any two of the equations (3.5), yielding

$$\begin{aligned}\cot \theta &= \frac{f(n_2)(f(n_1) - 1) \cot(\pi n_1/N) - f(n_1)(f(n_2) - 1) \cot(\pi n_2/N)}{(f(n_2) - f(n_1))}, \\ \cot \phi &= \frac{(f(n_1) - 1) \cot(\pi n_1/N) - (f(n_2) - 1) \cot(\pi n_2/N)}{(f(n_2) - f(n_1))},\end{aligned}\quad (3.8)$$

which expresses θ and ϕ in terms of the weights W .

Using the integrability condition (2.22) we find

$$\Omega \overline{\Omega} = 1, \quad (3.9)$$

with

$$\Omega^{-1} = \sin(\pi/N) (\cot(\phi - \theta) - \cot(\pi/N)) \quad (3.10)$$

and a similar equation for $\overline{\Omega}$. Since we have expressed θ and ϕ in terms of the ratios of weights $f(n)$ and similarly $\overline{\theta}$ and $\overline{\phi}$ in terms of the $\overline{f}(n)$, we can substitute (3.8) into (3.10); then (3.9) gives a relation relating the W and \overline{W} weights.

For $N = 3$, (3.9) and (3.10) are the same equations that we presented elsewhere without derivation,⁽¹⁰⁾ except for a slight change of notation, as K and Δ in the earlier work are changed to $2K_1$ and Δ_1 here. These equations are useful to check whether a particular model is integrable or not. Yet even in the $N = 3$ case, we find it more convenient to use the parameters θ and ϕ instead. Moreover, even though we can in principle use the equations (3.5) to calculate the K_j and Δ_j for $j \geq 2$ in terms of K_1 and Δ_1 and (3.9) and (3.10) for the relations between the K_j and Δ_j and the \overline{K}_j and $\overline{\Delta}_j$, we have found out that these algebraic equations become more and more complex to solve, as N increases. In the next subsections, we shall present an alternative way.

3.2. Interaction Energy Parameters of Chiral Potts Model

We may rewrite (2.13) in terms of the variables θ and ϕ as

$$\frac{W(n)}{W(n-1)} = \left(\frac{\sin(N\phi)}{\sin(N\theta)} \right)^{1/N} \frac{\sin(\theta + \pi n/N)}{\sin(\phi + \pi n/N)}. \quad (3.11)$$

Together with (2.2) and (2.5), we find

$$-\frac{\mathcal{E}(n) - \mathcal{E}(n-1)}{k_B T} = \log \frac{W(n)}{W(n-1)} = A + B_n = \sum_{j=1}^{N-1} r_j \omega^{jn}, \quad (3.12)$$

with

$$A = \frac{1}{N} \log \frac{\sin(N\phi)}{\sin(N\theta)}, \quad B_n = \log \frac{\sin(\theta + \pi n/N)}{\sin(\phi + \pi n/N)}, \quad (3.13)$$

$$r_j = -\frac{E_j}{k_B T} (1 - \omega^{-j}). \quad (3.14)$$

The Fourier coefficients r_j in (3.12) can now be written as

$$Nr_0 = NA + \sum_{n=1}^N B_n = 0, \quad r_j = N^{-1} \sum_{n=1}^N \omega^{-nj} B_n. \quad (3.15)$$

Consequently, we find from (3.14) and (2.11) that

$$K_j \omega^{\Delta_j} = \frac{r_j}{1 - \omega^{-j}} = -\frac{S_j + iC_j}{2N \sin(\pi j/N)}, \quad (3.16)$$

where

$$S_j = \sum_{n=1}^N B_n \sin\left((2n-1)j \frac{\pi}{N}\right), \quad C_j = \sum_{n=1}^N B_n \cos\left((2n-1)j \frac{\pi}{N}\right). \quad (3.17)$$

Using (3.16) we obtain

$$\Delta_j = \frac{N}{2\pi} \arctan \frac{C_j}{S_j}, \quad K_j = \frac{(S_j^2 + C_j^2)^{1/2}}{2N \sin(\pi j/N)}. \quad (3.18)$$

To have $\Delta_j = 0$, we must choose θ and ϕ such that $C_j = 0$. From (3.17) and (3.13), we find if $\theta + \phi = -\pi/N$, then $B_n = -B_{N-n+1}$ and $C_j, \Delta_j = 0$.

3.3. Alternative Approach

Even though the results in the previous subsection suffice, for future reference it may be useful to provide more explicit formulae using a normalization first used by Baxter.⁽³⁷⁾

If the average energy for a bond is to be zero, the natural normalization is

$$\prod_{n=0}^{N-1} W(n) = 1. \quad (3.19)$$

We may then rewrite the $W(n)$ in (2.13) in terms of the variables θ and ϕ given in (3.3) explicitly as

$$W(n) = \prod_{m=0}^{N-1} f_m^{\alpha_{m,n}}, \quad (3.20)$$

where

$$f_m \equiv \frac{\sin(\theta + \frac{m\pi}{N})}{\sin(\phi + \frac{m\pi}{N})} = \exp(B_m), \quad (3.21)$$

$$\alpha_{m,n} \equiv \frac{1}{2} \text{sign}(n + \frac{1}{2} - m) - \frac{(n + \frac{1}{2} - m)}{N}, \quad (3.22)$$

$$\log W(n) = \sum_{m=0}^{N-1} \alpha_{m,n} \log f_m \equiv -\frac{\mathcal{E}(n)}{k_B T}, \quad (3.23)$$

also using the identity

$$\sin(N\theta) = 2^{N-1} \prod_{n=0}^{N-1} \sin\left(\theta + \frac{n\pi}{N}\right). \quad (3.24)$$

It is easy to show, replacing ω by x and then taking the limit $x \rightarrow \omega$, that

$$\sum_{n=0}^{N-1} \alpha_{m,n} \omega^{np} = \begin{cases} 0, & \text{if } p = 0, \\ \frac{\omega^{mp}}{1 - \omega^p}, & \text{if } p \neq 0, \end{cases} \quad (3.25)$$

and its inverse is

$$\sum_{p=1}^{N-1} \frac{\omega^{-np}}{N} \frac{\omega^{mp}}{1 - \omega^p} = \alpha_{m,n}. \quad (3.26)$$

We can then rewrite

$$\mathcal{E}(n) = -k_B T \log W(n) = -\frac{1}{\beta} \sum_{m=0}^{N-1} \alpha_{m,n} \log f_m = \sum_{l=1}^{N-1} E_l \omega^{ln}, \quad (3.27)$$

with

$$E_l = \frac{1}{N} \sum_{n=0}^{N-1} \mathcal{E}(n) \omega^{-ln}, \quad E_0 \equiv 0, \quad (3.28)$$

see also (2.2), together with the inverse results

$$E_l = -\frac{1}{\beta N} \sum_{m=0}^{N-1} \frac{\omega^{-ml}}{1 - \omega^{-l}} \log f_m = -\frac{\omega^{(2l-N)/4}}{2\beta N \sin \frac{\pi l}{N}} \sum_{m=0}^{N-1} \omega^{-ml} \log f_m, \quad (3.29)$$

$$E_{N-l} = E_l^*, \quad E_N \equiv E_0 = 0. \quad (3.30)$$

These results also agree with (3.16) of the previous subsection.

3.4. Superwetting in the Ground State

Let us say that the interface is superwet at $T = 0$, if we can find a suitable relabeling of the state differences n such that

$$\mathcal{E}(n) - \mathcal{E}(0) = n(\mathcal{E}(1) - \mathcal{E}(0)) > 0, \quad n = 0, \dots, N-1. \quad (3.31)$$

This is equivalent to the second-order difference equation

$$\mathcal{E}(m+1) - 2\mathcal{E}(m) + \mathcal{E}(m-1) = 0, \quad m = 1, \dots, N-2. \quad (3.32)$$

Imposing the condition, see also (3.19),

$$\sum_{n=0}^{N-1} \mathcal{E}(n) = 0, \quad (3.33)$$

we can solve these conditions, in terms of one constant C , by

$$\mathcal{E}(n) = -2NC \alpha_{0,n} = -C(N - 2n - 1), \quad C > 0, \quad (3.34)$$

together with its Fourier coefficients

$$E_l = -C \frac{\omega^{(2l-N)/4}}{\sin(\pi l/N)} = E_{N-l}^*, \quad l = 1, \dots, N-1, \quad (3.35)$$

where we have used (3.22) and (3.25). We note that the results (3.34) and (3.35) correspond also to the zero-temperature superintegrable⁽³²⁾ chiral Potts model and its corresponding quantum chain.⁽²⁶⁾

4. INTEGRABLE THREE-STATE CHIRAL CLOCK MODEL

In this section, we take a closer look at the 3-state integrable chiral clock models. For $N = 3$, we use the chiral clock representation (2.12) to write the Boltzmann weights as

$$\begin{aligned} W(n) &= \exp \left[2K_1 \cos \left(\frac{2\pi}{3}(n + \Delta_1) \right) \right], \\ \overline{W}(n) &= \exp \left[2\overline{K}_1 \cos \left(\frac{2\pi}{3}(n + \overline{\Delta}_1) \right) \right]. \end{aligned} \quad (4.1)$$

Letting

$$w_n = W(-n)/W(0), \quad \overline{w}_n = \overline{W}(-n)/\overline{W}(0). \quad (4.2)$$

and writing $K = 2K_1$ and $\overline{K} = 2\overline{K}_1$, we find from (4.1),

$$w_2/w_1 = \exp[-\sqrt{3}K \sin(2\pi\Delta/3)], \quad w_2w_1 = \exp[-3K \cos(2\pi\Delta/3)], \quad (4.3)$$

where we have dropped the subscript 1 in Δ . Consequently, we find

$$K = 2K_1 = \frac{1}{3} \sqrt{\log^2(w_1w_2) + 3 \log^2(w_2/w_1)} \quad (4.4)$$

and

$$\Delta = \Delta_1 = \frac{3}{2\pi} \arctan \left(\frac{\sqrt{3} \log(w_2/w_1)}{\log(w_1w_2)} \right). \quad (4.5)$$

From (2.21), we find

$$\begin{aligned} w_1 \equiv w_1(\theta, \phi) &= \left[\frac{\sin^2(\phi) \sin(\theta + \frac{1}{3}\pi) \sin(\theta + \frac{2}{3}\pi)}{\sin^2(\theta) \sin(\phi + \frac{1}{3}\pi) \sin(\phi + \frac{2}{3}\pi)} \right]^{1/3}, \\ w_2 \equiv w_2(\theta, \phi) &= \left[\frac{\sin(\phi) \sin^2(\theta + \frac{1}{3}\pi) \sin(\phi + \frac{2}{3}\pi)}{\sin(\theta) \sin^2(\phi + \frac{1}{3}\pi) \sin(\theta + \frac{2}{3}\pi)} \right]^{1/3}. \end{aligned} \quad (4.6)$$

Similar relations hold for \overline{K} , $\overline{\Delta}$, \overline{w}_1 , and \overline{w}_2 in terms of $\overline{\theta}$ and $\overline{\phi}$.

4.1. Ferromagnetic regions

We want to determine for which values of θ and ϕ the (relative) Boltzmann weights are positive real and in the ferromagnetic regime. This means that

we have to look for a suitable fundamental domain as the relative Boltzmann weights have a few simple symmetries: They are periodic modulo π in θ and ϕ ,

$$\begin{aligned} w_1(\theta + \pi, \phi) &= w_1(\theta, \phi + \pi) = w_1(\theta, \phi), \\ w_2(\theta + \pi, \phi) &= w_2(\theta, \phi + \pi) = w_2(\theta, \phi), \end{aligned} \quad (4.7)$$

they invert under the interchange of θ and ϕ ,

$$w_1(\phi, \theta) w_1(\theta, \phi) = 1, \quad w_2(\phi, \theta) w_2(\theta, \phi) = 1, \quad (4.8)$$

and there is a transformation interchanging w_1 and w_2 ,

$$w_1(\frac{2}{3}\pi - \phi, \frac{2}{3}\pi - \theta) = w_2(\theta, \phi), \quad w_2(\frac{2}{3}\pi - \phi, \frac{2}{3}\pi - \theta) = w_1(\theta, \phi). \quad (4.9)$$

After some work, one finds that modulo π the ferromagnetic regimes are given by

$$\begin{aligned} 0 \leq w_2 \leq w_1 \leq 1 \quad \text{for} \quad & -\frac{1}{3}\pi \leq \theta \leq \phi \leq -\frac{1}{3}\pi - \theta, \\ & \text{or} \quad \pi - \theta \leq \phi \leq \theta \leq \frac{2}{3}\pi, \end{aligned} \quad (4.10)$$

$$\begin{aligned} 0 \leq w_1 \leq w_2 \leq 1 \quad \text{for} \quad & -\frac{1}{3}\pi - \phi \leq \theta \leq \phi \leq 0, \\ & \text{or} \quad 0 \leq \phi \leq \theta \leq \frac{1}{3}\pi - \phi. \end{aligned} \quad (4.11)$$

Here, we can ignore the latter two choices (4.11) as they reduce to the first two choices (4.10) under the interchange transformation (4.9).

For the integrable 3-state chiral Potts model, we also need to require the integrability condition, see (2.22),

$$\phi + \bar{\phi} = \theta + \bar{\theta} + \frac{1}{3}\pi, \quad (\text{modulo } \pi). \quad (4.12)$$

Combining this with (4.10) above, we arrive at a unique fundamental domain

$$-\frac{1}{3}\pi \leq \theta \leq \phi \leq -\frac{1}{3}\pi - \theta, \quad -\frac{1}{3}\pi \leq \bar{\theta} \leq \bar{\phi} \leq -\frac{1}{3}\pi - \bar{\theta}, \quad (4.13)$$

where

$$\begin{aligned}
0 \leq w_2 = w_2(\theta, \phi) \leq w_1 = w_1(\theta, \phi) \leq 1, \\
0 \leq \bar{w}_2 = w_2(\bar{\theta}, \bar{\phi}) \leq \bar{w}_1 = w_1(\bar{\theta}, \bar{\phi}) \leq 1.
\end{aligned} \tag{4.14}$$

Note that the integrability condition (4.12) is fully compatible with the transformation (4.9), so that other orderings of w_1 and w_2 , and of \bar{w}_1 and \bar{w}_2 , correspond to equivalent domains.

4.2. Critical region

We now consider the case with

$$\bar{K} = K, \quad \bar{\Delta} = p\Delta. \tag{4.15}$$

Substituting (4.6) into (4.4) and (4.5), and using similar equations for the barred variables, one can rewrite (4.15) to give two conditions between the θ , ϕ , $\bar{\theta}$, and $\bar{\phi}$. As we also have (4.12), we find there is only one free parameter left.

At the Potts critical point, we find

$$\bar{K}_c = K_c = \frac{2}{3} \log(1 + \sqrt{3}) = 1.49245929 \dots, \quad \bar{\Delta} = \Delta = 0. \tag{4.16}$$

From (4.5) and (4.6), we see that for $\bar{\Delta} = p\Delta = 0$ to hold, we need to have

$$w_1 = w_2, \quad \bar{w}_1 = \bar{w}_2, \quad \text{or} \quad \theta + \phi = \frac{1}{3}\pi, \quad \bar{\theta} + \bar{\phi} = \frac{1}{3}\pi. \tag{4.17}$$

Now we use (4.4) and (4.17) to obtain

$$-\log w_1 = -\log \bar{w}_1 = \frac{3}{2}K_c, \quad \text{or} \quad \phi = \bar{\phi} = -\frac{1}{12}\pi, \quad \theta = \bar{\theta} = -\frac{1}{4}\pi. \tag{4.18}$$

Near the critical point, we can make the changes of variables

$$\begin{aligned}
\phi &= -\frac{1}{12}\pi - \delta\phi, & \theta &= -\frac{1}{4}\pi - \delta\theta, \\
\bar{\phi} &= -\frac{1}{12}\pi - \delta\bar{\phi}, & \bar{\theta} &= -\frac{1}{4}\pi - \delta\bar{\theta}, \\
\delta\bar{\theta} &= \delta\phi + \delta\bar{\phi} - \delta\theta.
\end{aligned} \tag{4.19}$$

Substituting these expansions into (4.6), and then using (4.4), (4.5), and (4.15), we find

$$\begin{aligned}
\delta\theta &= \delta\phi + (p^2 - 1)r_c \delta\phi^2 + (p^2 - 1)^2 r_c^2 \delta\phi^3 \\
&\quad + \frac{1}{12}(p^2 - 1) \left[(15p^4 - p^2(142 + 64\sqrt{3}) + 15) r_c^3 \right. \\
&\quad \left. + (p^2(250 + 122\sqrt{3}) - 174 - 78\sqrt{3}) r_c^2 \right. \\
&\quad \left. + (p^2(110 + 78\sqrt{3}) + 470 + 222\sqrt{3}) r_c \right. \\
&\quad \left. - (p^2 + 1)(261 + 171\sqrt{3}) \right] \delta\phi^4 + O(\delta\phi^5)
\end{aligned} \tag{4.20}$$

and

$$\begin{aligned}
\delta\bar{\phi} - p\delta\phi - \frac{1}{2}(p+1)(\delta\theta - \delta\phi) &= \delta\bar{\theta} - p\delta\phi - \frac{1}{2}(p-1)(\delta\theta - \delta\phi) \\
&= -\frac{1}{3}p(p^2 - 1) \left((14 + 8\sqrt{3}) r_c^2 - (53 + 25\sqrt{3}) r_c + 45 + 18\sqrt{3} \right) \\
&\quad \times \delta\phi^3 \left(1 + \frac{3}{2}(p^2 - 1) r_c \delta\phi \right) + O(\delta\phi^5),
\end{aligned} \tag{4.21}$$

where we have defined

$$r_c = \frac{1}{2}(1 + \sqrt{3}) \left(1 + \frac{7\sqrt{3} - 12}{\log(1 + \sqrt{3})} \right) = 1.535044409 \dots, \tag{4.22}$$

in order to simplify the first three orders in (4.20). One can also easily verify from (4.20) and (4.21) that $\delta\bar{\theta}$ expressed as a function of $\delta\bar{\phi}$ is of the form (4.20) with p replaced by $1/p$.

Substituting (4.20) and (4.21) back into (4.6) and using

$$K - K_c = -\frac{K_c t}{1 + t} \approx -K_c t, \quad \text{where} \quad t \equiv \frac{T - T_c}{T_c}, \tag{4.23}$$

we find from (4.4) and (4.5) that

$$K_c t = -\frac{1}{3}(p^2 + 1)(3 + \sqrt{3}) r_c \delta\phi^2 \left(1 + (p^2 - 1) r_c \delta\phi \right) + O(\delta\phi^4), \tag{4.24}$$

and

$$\Delta = \bar{\Delta}/p = \frac{3 - \sqrt{3}}{\pi K_c} \delta\phi \left(1 + \frac{1}{2}(p^2 - 1) r_c \delta\phi \right) + O(\delta\phi^3). \tag{4.25}$$

Eliminating $\delta\phi$ from the above equations we find, near the Potts critical point on the integrable curve, where $K = 2K_1 \approx K_c(1-t) = \frac{2}{3}\log(1+\sqrt{3})(1-t)$, the result

$$t = -C_t(1+p^2)\Delta^2 + O(t^2, t\Delta^2, \Delta^4),$$

$$C_t \equiv \frac{1}{18}\pi^2(2 + (7\sqrt{3} + 12)K_c) = 9.959616982\cdots, \quad (4.26)$$

Since the modulus k is given by (2.25), we can use (4.19) to (4.25) to express it in terms $t = T/T_c - 1$ as

$$k^2 = -C_k t + O(t^3), \quad C_k \equiv \frac{54(2 + \sqrt{3})K_c^2}{2 + (7\sqrt{3} + 12)K_c} = 4.981050242\cdots, \quad (4.27)$$

which is independent of p at this order.

The above expansions for the critical region include the symmetric case for $p = 1$ and the Ostlund-Huse model for $p = 0$. We do not have such universal formulae in the low-temperature regime, which we shall discuss next.

4.3. Low-Temperature Limit

Considering the three-state chiral clock model with $\overline{K} = K$ and $\overline{\Delta} = p\Delta$ in the low-temperature limit, we find that the limits $T \rightarrow 0$ and $p \rightarrow 0$ (or $p \rightarrow 1$) do not commute. The limit $p \rightarrow 0$ does not reproduce the Ostlund-Huse model ($p \equiv 0$) results, nor does the limit $p \rightarrow 1$ reproduce the symmetric model ($p \equiv 1$) results. We shall have to consider several regimes separately.

First, for $p \neq 0$ and $p \neq 1$, we let

$$\phi = -\frac{1}{3}\pi + \delta\phi, \quad \theta = -\frac{1}{3}\pi + \delta\theta, \quad \overline{\phi} = -\delta\overline{\phi}, \quad \overline{\theta} = -\frac{1}{3}\pi + \delta\overline{\theta}, \quad (4.28)$$

and we find the leading low-temperature expansion results

$$\delta\theta \approx \delta\phi \delta\psi \equiv \delta\phi \left(\frac{2}{\sqrt{3}} \delta\phi \right)^{\sqrt{b^2+b+1}}, \quad (4.29)$$

$$\delta\overline{\phi} \approx \delta\phi, \quad \delta\overline{\theta} \approx \delta\phi \left(\frac{2}{\sqrt{3}} \delta\phi \right)^{b-1}, \quad (4.30)$$

with

$$b = \frac{\sin(\frac{1}{6}(1+p)\pi)}{\sin(\frac{1}{6}(1-p)\pi)}, \quad \sqrt{b^2 + b + 1} = \frac{\frac{1}{2}\sqrt{3}}{\sin(\frac{1}{6}(1-p)\pi)}. \quad (4.31)$$

Then we see from (4.4) and (4.6) that

$$K = \overline{K} \approx -\frac{2}{3\sqrt{3}} \log \delta\psi \rightarrow \infty, \text{ as } \delta\phi \rightarrow 0, \quad (4.32)$$

whereas from (4.5) and (4.6) we find that $\overline{\Delta} = p\Delta$ and

$$\Delta \approx \frac{1}{4} + \frac{3\delta\phi}{2\pi \log \delta\psi} \approx \frac{1}{4} - \frac{1}{2\pi K} \exp \left[-3K \sin \left(\frac{1}{6}(1-p)\pi \right) \right]. \quad (4.33)$$

Further terms to the above asymptotic expansions follow by expanding $\delta\theta$, $\delta\overline{\phi}$, and $\delta\overline{\theta}$ in powers of $\delta\phi$, $\delta\psi \sim \delta\phi^{\sqrt{b^2+b+1}}$, $\delta\phi^{b-1}$, and $1/\log \delta\psi$. This can be done for $1 < b < \infty$, or $0 < p < 1$. For $b \rightarrow 1$ or $p \rightarrow 0$, $\delta\phi^{b-1} \rightarrow 1$ and is no longer small, so that different asymptotic expansions arise. For $b \rightarrow \infty$ or $p \rightarrow 1$, we still have $\phi \rightarrow \frac{1}{3}\pi$ and $\overline{\phi} \rightarrow 0$, so that there is still another regime at $p \approx 1$ between the above regime and the symmetric case $p \equiv 1$.

For the three-state Ostlund-Huse case we have $p \equiv \overline{\Delta} \equiv 0$, so that

$$\overline{\theta} + \overline{\phi} = -\frac{1}{3}\pi, \quad \frac{\sin(3\overline{\theta})}{\sin(3\overline{\phi})} = 1. \quad (4.34)$$

Using also (4.13), we can then solve $\overline{\theta}$ and $\overline{\phi}$ in terms of θ and ϕ , namely

$$\overline{\theta} = -\frac{1}{3}\pi - \frac{1}{2}(\theta - \phi), \quad \overline{\phi} = \frac{1}{2}(\theta - \phi). \quad (4.35)$$

In the low-temperature limit, with ϕ and θ near $-\frac{1}{3}\pi$,

$$\phi = -\frac{1}{3}\pi + \delta\phi, \quad \theta = -\frac{1}{3}\pi + \delta\theta, \quad (4.36)$$

we can find in a systematic way, from $K = \overline{K}$, the asymptotic expansion for $\delta\theta$ in terms of powers of $\delta\phi$, $\delta\phi^{\sqrt{3}}$, and $1/\log \delta\phi$, in agreement with what one would expect from (4.30) and (4.31) with $b-1=0$. The asymptotic expansion so obtained can be equivalently (and more economically) expressed as

$$\begin{aligned}
\log \delta\theta &= \log(\delta\phi \delta\tilde{\psi}) + \frac{1}{2}\delta\phi - \sqrt{3}\delta\tilde{\psi} \\
&+ \left(\frac{4+\sqrt{3}}{8} - \frac{1}{2l_\psi}\right)\delta\phi^2 - \frac{1+\sqrt{3}}{2}\delta\phi\delta\tilde{\psi} + \frac{6-\sqrt{3}}{2}\delta\tilde{\psi}^2 \\
&+ \left(\frac{1}{18} + \frac{1}{4l_\psi^2}\right)\delta\phi^3 - \left(\frac{5+7\sqrt{3}}{8} - \frac{2+\sqrt{3}}{2l_\psi} + \frac{\sqrt{3}}{2l_\psi^2}\right)\delta\phi^2\delta\tilde{\psi} \\
&+ \frac{6+\sqrt{3}}{2}\delta\phi\delta\tilde{\psi}^2 + \frac{27-29\sqrt{3}}{6}\delta\tilde{\psi}^3 + \dots, \tag{4.37}
\end{aligned}$$

where

$$l_\psi \equiv \log \delta\tilde{\psi} = \sqrt{3} \log(\delta\phi/\sqrt{3}), \quad \delta\tilde{\psi} \equiv (\delta\phi/\sqrt{3})^{\sqrt{3}}. \tag{4.38}$$

Therefore the leading order is

$$\delta\theta \approx \delta\phi \delta\tilde{\psi} \sim \delta\phi^{1+\sqrt{3}}, \tag{4.39}$$

which is quoted below (2.66) in subsection 2.6. Now (4.4) to (4.6) can be used to give

$$K = -\frac{2}{9}\sqrt{3}\log \delta\tilde{\psi} + \dots, \quad \Delta = \frac{1}{4} - \frac{1}{K\pi}e^{-3K/2} + \dots, \tag{4.40}$$

which was plotted as line 3 in Fig. 7b.

For the symmetric case with $p \equiv 1$, the low-temperature limit is given by

$$\theta \equiv \bar{\theta} = -\frac{1}{3}\pi + \delta\theta, \quad \phi \equiv \bar{\phi} = \theta + \frac{1}{6}\pi = -\frac{1}{6}\pi + \delta\theta, \tag{4.41}$$

with $\delta\theta \rightarrow 0$. We find from (4.4) to (4.6), the asymptotic expansion

$$K = -\frac{2}{9}\sqrt{3}\log \delta\theta + \dots, \quad \Delta = \frac{1}{4} - \frac{\log 2}{2\pi K} + \dots, \tag{4.42}$$

which was plotted as line 1 in Fig. 7b. Thus Δ decreases from $\frac{1}{4}$ linearly as T increases from zero, which is a behavior very different from that shown in (4.42) for the Ostlund-Huse case, or from (4.33).

The symmetric case can be extended by replacing the products in (2.54), in leading order, by their limiting values and assuming that the front factors, which are powers of $1/\Lambda$ and $1/\bar{\Lambda}$, are small. The weights then take on the

form (2.59), which was also considered by Baxter. We shall call this case the “quasi-symmetric” case. More precisely, with

$$\theta = -\frac{1}{3}\pi + \delta\theta, \quad \bar{\theta} = -\frac{1}{3}\pi + \delta\bar{\theta}, \quad \phi \rightarrow \phi_0 \neq 0 \text{ or } -\frac{1}{3}\pi, \quad (4.43)$$

we find from (4.13) that

$$\bar{\phi} = -\frac{1}{3}\pi - \phi + \delta\theta + \delta\bar{\theta} \rightarrow -\frac{1}{3}\pi - \phi_0. \quad (4.44)$$

Now, if we let

$$g \equiv \frac{\sin^2(\frac{1}{3}\pi - \phi_0)}{\sin(\frac{1}{3}\pi) \sin(\frac{1}{3}\pi + \phi_0) \sin(-\phi_0)}, \quad (4.45)$$

and

$$s \equiv -\log \frac{\sin(-\phi_0)}{\sin(\frac{1}{3}\pi - \phi_0)}, \quad \bar{s} \equiv -\log \frac{\sin(\frac{1}{3}\pi + \phi_0)}{\sin(\frac{1}{3}\pi - \phi_0)}, \quad (4.46)$$

then we find from (4.6) for $\delta\theta$ and $\delta\bar{\theta}$ small, the simple formulae

$$w_n \approx e^{-s} (g \delta\theta)^{n/3}, \quad \bar{w}_n \approx e^{-\bar{s}} (g \delta\bar{\theta})^{n/3}, \quad \text{for } n = 1 \text{ or } 2. \quad (4.47)$$

Here we have ignored terms that are one order higher in $\delta\theta$ or $\delta\bar{\theta}$. If we substitute (4.47) in (4.4) and (4.5), we find

$$K \approx \frac{1}{3} \sqrt{(u + 2s)^2 + \frac{1}{3}u^2}, \quad \bar{K} \approx \frac{1}{3} \sqrt{(\bar{u} + 2\bar{s})^2 + \frac{1}{3}\bar{u}^2}, \quad (4.48)$$

$$\Delta \approx \frac{3}{2\pi} \arctan \frac{\tan(\frac{1}{6}\pi) u}{u + 2s}, \quad \bar{\Delta} \approx \frac{3}{2\pi} \arctan \frac{\tan(\frac{1}{6}\pi) \bar{u}}{\bar{u} + 2\bar{s}}, \quad (4.49)$$

where

$$u \equiv -\log(g \delta\theta), \quad \bar{u} \equiv -\log(g \delta\bar{\theta}). \quad (4.50)$$

Formulae (4.48) and (4.49) are correct up to exponentially small corrections in the temperature T , as we have ignored terms of order $\delta\theta$ and $\delta\bar{\theta}$. Therefore,

$$u = \frac{1}{2} \sqrt{27K^2 - 3s^2} - \frac{3}{2}s + \text{exponentially small}, \quad (4.51)$$

and a similar equation with u , K , and s replaced by \bar{u} , \bar{K} , and \bar{s} . Expanding these to a few orders in $1/K$ and $1/\bar{K}$, we find

$$u = \frac{3}{2}\sqrt{3} K - \frac{3}{2}s - \frac{1}{12}\sqrt{3} \frac{s^2}{K} + \mathcal{O}\left(\frac{s^4}{K^3}\right), \quad (4.52)$$

and a similar equation with bars for \bar{u} . Substituting (4.52) into (4.49), we find

$$\begin{aligned}\Delta &= \frac{1}{4} - \frac{s}{2\pi K} - \frac{s^3}{108\pi K^3} + O\left(\frac{s^5}{K^5}\right), \\ \bar{\Delta} &= \frac{1}{4} - \frac{\bar{s}}{2\pi \bar{K}} - \frac{\bar{s}^3}{108\pi \bar{K}^3} + O\left(\frac{\bar{s}^5}{\bar{K}^5}\right).\end{aligned}\tag{4.53}$$

These again exhibit linear behavior in T , as in the symmetric case. In fact, for $\phi = \bar{\phi} = \frac{1}{6}\pi$ and $\theta = \bar{\theta}$, we have $s = \bar{s} = \log 2$, so (4.53) reduces smoothly to (4.42).

On the other hand, when $\phi \rightarrow -\frac{1}{3}\pi$, $\bar{\phi} \rightarrow 0$, we have $s \rightarrow 0$ and $\bar{s} \rightarrow \infty$. Then Δ tends to $\frac{1}{4}$ extremely fast, whereas $\bar{\Delta}$ tends to $\frac{1}{4}$ very slowly. In the limit, there is a crossover from the linear behavior of (4.53) to the exponential behavior of the first low-temperature regime described by (4.28) to (4.33).

Finally, solving ϕ_0 from $\bar{s} = \gamma s$ and $\bar{\theta}$ from $\bar{u} = \gamma u$, we find from (4.48) and (4.49) that $\bar{K} = \gamma K$ and $\bar{\Delta} = \Delta$ to all algebraic orders in T . So the quasi-symmetric case is closely related to integrable 3-state chiral clock models with symmetric chiral field, $\bar{\Delta} \equiv \Delta$, and we can use this as a definition, suitable also outside the low-temperature regime.

5. SYMMETRIC N -STATE CHIRAL POTTS MODEL

In this section we study the symmetric case for general N and give graphs for the chiral clock model parameters.

5.1. Symmetric Lattice

For the symmetric case with $W = \bar{W}$, the integrability condition (2.18) or (2.22) becomes

$$\phi = \theta + \frac{\pi}{2N}.\tag{5.1}$$

Substituting this equation into (3.13), we find from (3.17) and (3.18) that K_j and Δ_j depend on only one parameter θ . We only need to study the regime (fundamental domain) with

$$-\frac{\pi}{N} \leq \theta \leq -\frac{3\pi}{4N}.\tag{5.2}$$

First, we can see from (3.13) that if we let $\theta \rightarrow \theta + \pi/N$, then $B_n \rightarrow B_{n+1}$. Consequently, combining the first part of (3.16) and the second equation of (3.15), we find that $K_j \omega^{\Delta_j} \rightarrow \omega^j K_j \omega^{\Delta_j}$. This means that by shifting the domain to $0 \leq \theta \leq \frac{1}{4}\pi/N$, the amplitudes K_j remain unchanged but $\Delta_j \rightarrow \Delta_j + j$. Secondly, we note the reflection symmetry $\theta \rightarrow -\theta - \frac{1}{2}\theta/N$, changing $B_n \rightarrow -B_{-n}$. Thus we can shift the domain to $-\frac{3}{4}\pi/N \geq \theta \geq -\frac{1}{2}\pi/N$, with the amplitudes K_j remaining unchanged but now $\Delta_j \rightarrow -\Delta_j$. Finally, for $-\frac{1}{2}\pi/N \leq \theta \leq 0$ (modulo π/N) the Boltzmann weights are not all positive, as can be seen easily from (3.11) or (3.20), with condition (5.1).

For $\theta \downarrow -\pi/N$, we can see from (3.13) that $B_1 \rightarrow -\infty$, hence $K_j \rightarrow \infty$ and temperature $T \rightarrow 0$. From (3.15) and (3.16) we find

$$K_j \omega^{\Delta_j} \rightarrow \frac{B_1}{N(\omega^j - 1)}. \quad (5.3)$$

Since the ratios are finite, we obtain the zero-temperature results

$$\omega^{2\Delta_j} = -\omega^{-j}, \quad \Delta_j = \frac{1}{4}(N - 2j), \quad \frac{K_j}{K_1} = \frac{\sin(\pi/N)}{\sin(\pi j/N)}. \quad (5.4)$$

Comparing with (3.35) we see that we are at a superwetting point.

For the other end of the fundamental domain,

$$\theta = \theta_{\text{FZ}} \equiv -\frac{3\pi}{4N}, \quad (5.5)$$

we find using (3.13) that $B_n = -B_{N-n+1}$. Hence, we conclude from (3.17) that $C_j = 0$, or $\Delta_j = 0$. In fact, by putting $\theta = \theta_{\text{FZ}} - \lambda$, it is easy to show that $B_n(\lambda) \rightarrow -B_{N-n+1}(-\lambda)$ for $\lambda \rightarrow -\lambda$. Consequently, from (3.17) we find that the S_j are unchanged but $C_j \rightarrow -C_j$, as $\lambda \rightarrow -\lambda$. This means that the K_j are unchanged, but the Δ_j flip signs as λ changes its sign.

To summarize, we find, as we increase θ from $-\pi/N$, that the integrable line plotted as a function of $1/K_j$ versus Δ_j starts from the zero-temperature values given in (5.4) and the Δ_j decrease and the $1/K_j$ increase and for $\theta = \theta_{\text{FZ}}$, we have $\Delta_j = 0$ and the $1/K_j$ reach their maximum values,

$$K_{jc} = \frac{1}{N \sin(\pi j/N)} \sum_{n=1}^{\lfloor \frac{1}{2}N \rfloor} \sin\left((2n-1)\frac{j\pi}{N}\right) \log \frac{\sin\left((n - \frac{1}{4})\pi/N\right)}{\sin\left((n - \frac{3}{4})\pi/N\right)}. \quad (5.6)$$

This corresponds to the symmetric case of the Fateev-Zamolodchikov self-dual solution, and is therefore critical. Needless to say that (5.6) gives the critical temperature for the symmetric solvable chiral Potts model. As θ increases further the values of Δ_j are now negative. The curves are symmetric with respect to the vertical axis.

5.2. Graphs for Integrable Symmetric Case with $N=4, \dots, 7$

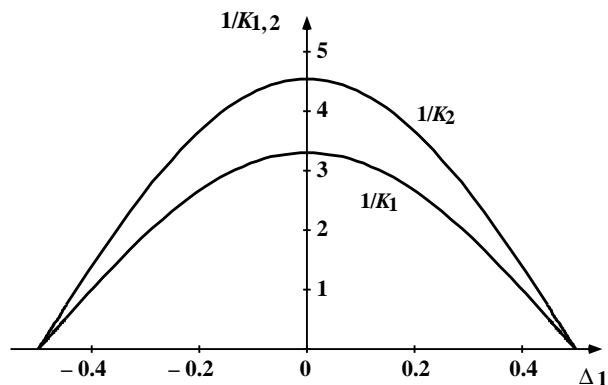


Fig. 8a. The 4-state chiral Potts model: $1/K_1$ and $1/K_2$ versus Δ_1 .

For $N = 4$, using (2.12), we have

$$-\frac{\mathcal{E}(n)}{k_B T} = 2K_1 \cos\left(\frac{2\pi}{N}(jn + \Delta_1)\right) + K_2 (-1)^n. \quad (5.7)$$

In Fig. 8a we plot $1/K_1$ and $1/K_2$ versus Δ_1 and in Fig. 8b we plot $1/K_2$ versus $1/K_1$, which is almost a straight line with slope approximately given by $\sqrt{2} \sim 1.41$. At temperature $T = 0$, we have from (5.4) that $\Delta_1 = \frac{1}{2}$ and $K_2/K_1 = \frac{1}{2}\sqrt{2}$. Therefore, if we let $k_B T K_1 = 1$ in the limit $T \rightarrow 0$ by a suitable choice of units, then the energies (5.7) for the different states are

$$\begin{aligned} \mathcal{E}(0) &= -\frac{3}{2}\sqrt{2}, & \mathcal{E}(1) &= \frac{3}{2}\sqrt{2}, \\ \mathcal{E}(2) &= \frac{1}{2}\sqrt{2}, & \mathcal{E}(3) &= -\frac{1}{2}\sqrt{2}. \end{aligned} \quad (5.8)$$

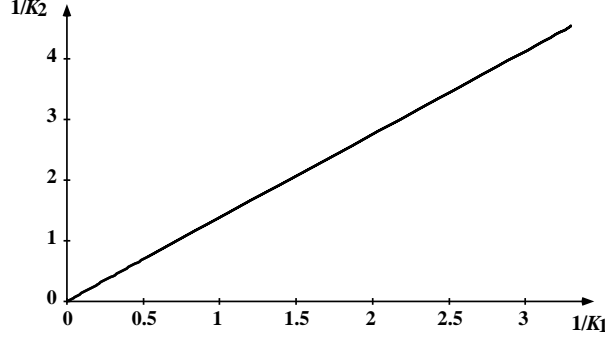


Fig. 8b. $N = 4$: $1/K_2$ versus $1/K_1$.

Hence, $\mathcal{E}(-n) - \mathcal{E}(0) = n\sqrt{2}$. This means that at zero temperature the integrable line is at a superwetting transition. As T or $1/K_j$ increases, Δ_1 decreases. When $\Delta_1 = 0$, we find from (5.6) that

$$K_{1c} = 0.3029227993, \quad K_{2c} = 0.2203433968, \quad K_{2c}/K_{1c} = 0.7273912604. \quad (5.9)$$

Comparing with the ratio $K_2/K_1 = \frac{1}{2}\sqrt{2}$ at zero temperature, we know that the curve in Fig. 8b is not a straight line. We may magnify the effect by plotting in Fig. 8c the ratio K_2/K_1 versus Δ_1 and indeed we find it not to be constant, with $\kappa_{jc} \lesssim 0.02$ for κ_j defined in (2.28).

For different N , we find more or less the same situation as for $N = 4$. For N odd, there are equal numbers of K_j and Δ_j with $1 \leq j \leq \frac{1}{2}(N-1)$. At $T = 0$, we find then from (5.4) that $\Delta_{\frac{1}{2}(N-1)} = \frac{1}{4}$ is the smallest of the Δ_j . For even N , there are $\frac{1}{2}N$ different amplitudes K_j and $\frac{1}{2}N - 1$ angles Δ_j , not counting $\Delta_{\frac{1}{2}N} \equiv 0$. Now at $T = 0$, $\Delta_{\frac{1}{2}N-1} = \frac{1}{2}$ is the smallest.

Again without loss of generality we can let $k_B T K_1 = 1$. Then at $T = 0$, we have

$$\mathcal{E}(n) = \sum_{j=1}^{N-1} \frac{\sin(\pi/N)}{\sin(\pi j/N)} \sin\left((2n-1)\frac{\pi j}{N}\right). \quad (5.10)$$

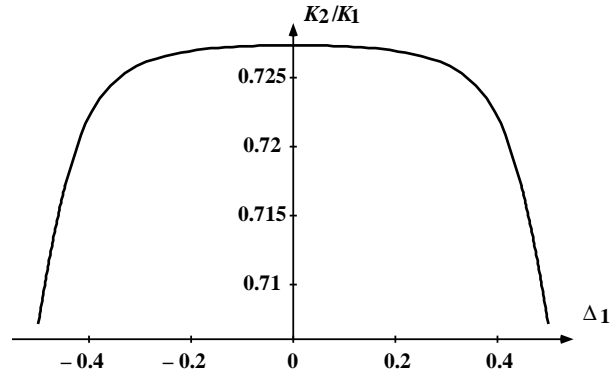


Fig. 8c. $N = 4$: K_2/K_1 versus Δ_1 .

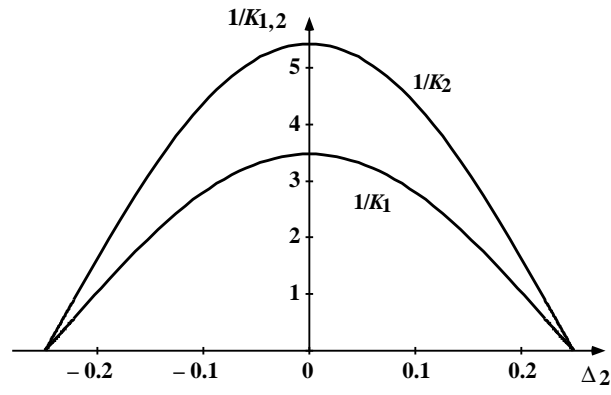


Fig. 9a. The 5-state chiral Potts model: $1/K_1$ and $1/K_2$ versus Δ_2 .

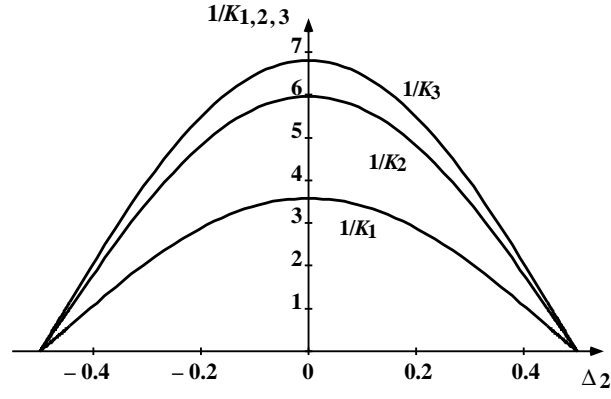


Fig. 10a. The 6-state chiral Potts model: $1/K_1$, $1/K_2$, and $1/K_3$ versus Δ_2 .

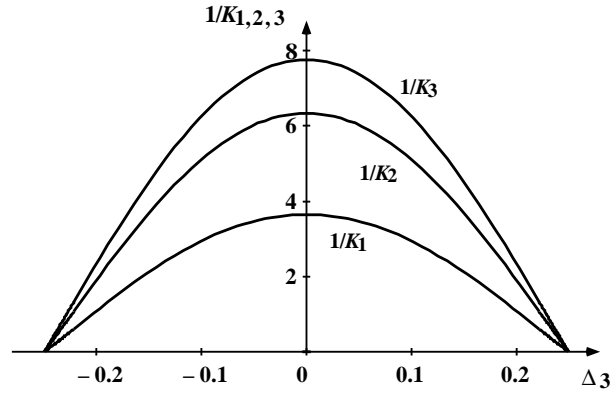


Fig. 11a. The 7-state chiral Potts model: $1/K_1$, $1/K_2$, and $1/K_3$ versus Δ_3 .

From this it is straightforward to show that

$$\mathcal{E}(-n) - \mathcal{E}(0) = 2n \sin(\pi/N). \quad (5.11)$$

It also follows by comparing (5.11) with (3.34) and (5.10) with (3.35). Hence, it is at the endpoint of a superwetting line. In Fig. 9a, (respectively 10a, or 11a), we plot $1/K_j$ with $1 \leq j \leq [\frac{1}{2}N]$ versus the smallest angle $\Delta_{[\frac{1}{2}(N-1)]}$ for $N = 5$, (6, or 7). In Fig. 9b, (10b, or 11b), we plot $1/K_j$ with $2 \leq j \leq [\frac{1}{2}N]$ versus $1/K_1$ for $N = 5$, (6, or 7). Again we find that the curves look very much like straight lines.

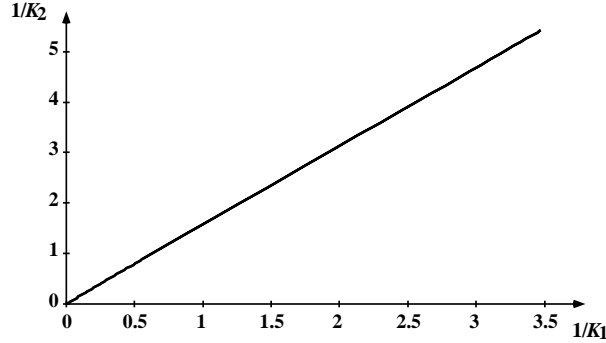


Fig. 9b. $N = 5$: $1/K_2$ versus $1/K_1$.

For $\theta = \theta_{\text{FZ}}$, we have $\Delta_j = 0$, and the K_j given by (5.6) have the numerical values

$$\begin{aligned} N = 5 : & \quad K_{1c} = 0.2878960239, \quad K_{2c} = 0.1845136297, \\ N = 6 : & \quad K_{1c} = 0.2793167217, \quad K_{2c} = 0.1675087565, \quad K_{3c} = 0.1468955978, \\ N = 7 : & \quad K_{1c} = 0.2738160609, \quad K_{2c} = 0.1577390412, \quad K_{3c} = 0.1288523620, \end{aligned} \quad (5.12)$$

which are the critical-temperature values. The ratios are given by

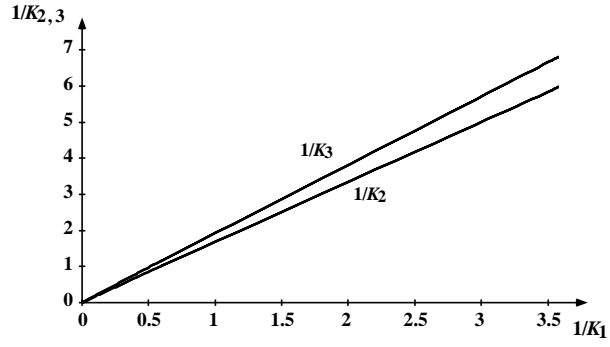


Fig. 10b. $N = 6$: $1/K_2$ and $1/K_3$ versus $1/K_1$.

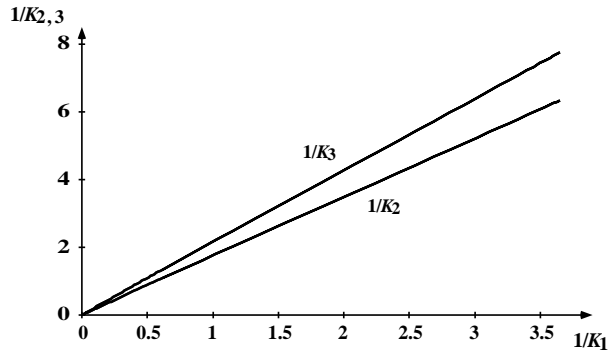


Fig. 11b. $N = 7$: $1/K_2$ and $1/K_3$ versus $1/K_1$.

$$\begin{aligned}
N = 5 : & \quad K_{2c}/K_{1c} = 0.6409037097, \\
N = 6 : & \quad K_{2c}/K_{1c} = 0.5997090164, \quad K_{3c}/K_{1c} = 0.5259105038, \\
N = 7 : & \quad K_{2c}/K_{1c} = 0.5760766578, \quad K_{3c}/K_{1c} = 0.4705800001. \quad (5.13)
\end{aligned}$$

Comparing these numbers with the ratios at zero temperature,

$$\begin{aligned}
N = 5 : & \quad K_2/K_1 = 0.6180339887, \\
N = 6 : & \quad K_2/K_1 = 0.5773502692, \quad K_3/K_1 = 0.5, \\
N = 7 : & \quad K_2/K_1 = 0.5549581321, \quad K_3/K_1 = 0.4450418679, \quad (5.14)
\end{aligned}$$

we find that the curves are not really straight lines.

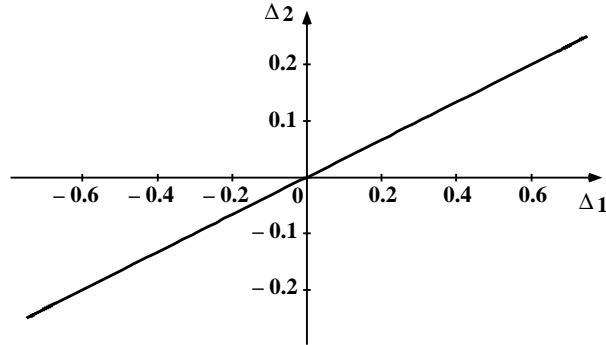


Fig. 9c. $N = 5$: Δ_2 versus Δ_1 .

In Fig. 9c, (10c, or 11c), the Δ_j for $N = 5$, (6, or 7) with $2 \leq j \leq [\frac{1}{2}N]$ are plotted versus Δ_1 . These curves also look like straight lines. In Fig. 9d we have plotted the ratio K_2/K_1 versus Δ_2 , while in Fig. 9e, we have plotted the ratio Δ_1/Δ_2 versus Δ_2 , both for $N = 5$. Again we find the ratios not to be exactly constant, with $\kappa_j, \delta_j \lesssim 0.02$.

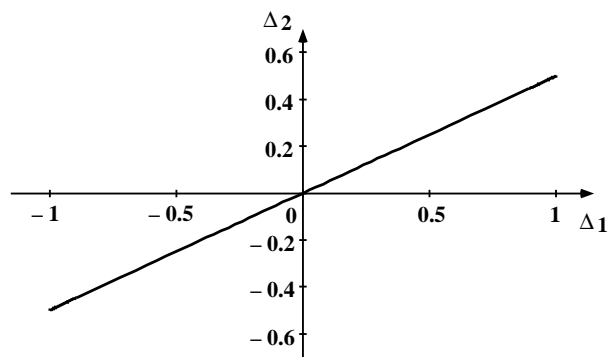


Fig. 10c. $N = 6$: Δ_2 versus Δ_1 .

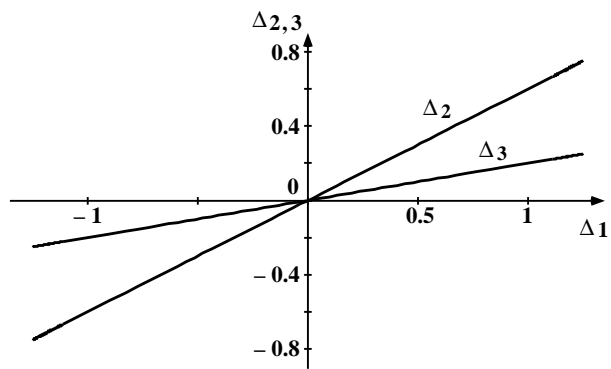


Fig. 11c. $N = 7$: Δ_2 and Δ_3 versus Δ_1 .

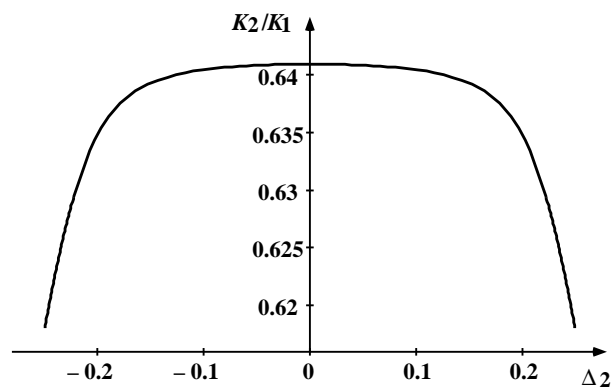


Fig. 9d. $N = 5$: K_2/K_1 versus Δ_2 .

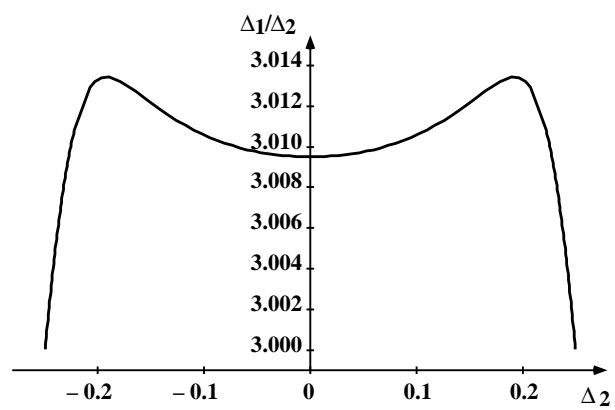


Fig. 9e. $N = 5$: Δ_1/Δ_2 versus Δ_2 .

6. LOW T BETHE ANSATZ FOR DIAGONAL INTERFACES

In this section we shall present our Bethe Ansatz calculations with free boundary conditions¹² for interfacial tensions of diagonal interfaces in the low-temperature limit, using an extension of the Bethe Ansatz⁽¹²⁾ similar to the ones introduced by Gaudin.⁽⁵⁸⁾ These calculations also confirm our dilogarithmic integral conjecture (2.76) for the entropic corrections (linear in the temperature T) to the ground-state interfacial tension results.

Using Baxter's notation,^(38,39) we start with the two coupled eigenvalue equations

$$\mathbf{T}_q \cdot \mathbf{y} = T_q \mathbf{x}, \quad \hat{\mathbf{T}}_q \cdot \mathbf{x} = \hat{T}_q \mathbf{y}, \quad (6.1)$$

where \mathbf{T}_q and $\hat{\mathbf{T}}_q$ are the two different diagonal transfer matrices. We solve this pair of equations, by assuming

$$\begin{aligned} x_{n_1, \dots, n_r} &= g(n_1, \dots, n_r | \zeta_1, \dots, \zeta_r), \\ 1 &\leq n_1 \leq n_2 \leq \dots \leq n_r \leq L, \\ y_{n_1, \dots, n_r} &= g(n_1 + \tfrac{1}{2}, \dots, n_r + \tfrac{1}{2} | \zeta_1, \dots, \zeta_r), \\ 1 &\leq n_1 \leq n_2 \leq \dots \leq n_r \leq L - 1, \end{aligned} \quad (6.2)$$

with a common function g which is a linear combination of exponentials. Here n_1, \dots, n_r stand for the positions of the interfaces in a given diagonal. We exclude overhangs, as in the Müller-Hartmann–Zittartz approximation,⁽⁵¹⁾ which is asymptotically exact at low temperatures. If a sequence of, say, m positions coincide, or $n_j = \dots = n_{j+m-1}$, then the interfaces merge to a single m -step interface. The ζ_1, \dots, ζ_r are complex parameters, also often written as $\zeta_j = \exp(ik_j)$. In terms of these, the eigenvalues are

$$T_q = \hat{T}_q = (w_1 \bar{w}_1)^{r/2} \prod_{j=1}^r (\zeta_j^{-1/2} + \zeta_j^{1/2}). \quad (6.3)$$

¹²Choosing fixed boundary conditions for the spins in the first and last rows, corresponds to free boundary conditions for the domain walls which live on the dual lattice, which is equivalent to demanding that a domain wall can not move outside the system as is expressed in (6.8) and (6.9) below.

From these, we can calculate the interfacial tension per two bonds via

$$\epsilon_r = -k_B T \log(T_q \hat{T}_q), \quad (6.4)$$

in agreement with Baxter's normalization.

For the function g we choose the Bethe Ansatz form

$$\begin{aligned} g(m_1, \dots, m_r | \zeta_1, \dots, \zeta_r) \\ = \mathcal{N} \sum_{\varepsilon_1 = \pm 1} \cdots \sum_{\varepsilon_r = \pm 1} \prod_{j=1}^r (-\zeta_j)^{-\varepsilon_j/2} \prod_{1 \leq j < k \leq r} A(\zeta_j^{-\varepsilon_j}, \zeta_k^{\varepsilon_k})^{1/2} \\ \times \sum_{P \in S_r} \prod_{1 \leq j < k \leq r} A(\zeta_{Pj}^{\varepsilon_{Pj}}, \zeta_{Pk}^{\varepsilon_{Pk}})^{1/2} \prod_{j=1}^r \zeta_{Pj}^{\varepsilon_{Pj} m_j}, \end{aligned} \quad (6.5)$$

with the usual two-body scattering function

$$A(\zeta_1, \zeta_2) \equiv \frac{1 - 2\Delta_{6v} \zeta_2 + \zeta_1 \zeta_2}{1 - 2\Delta_{6v} \zeta_1 + \zeta_1 \zeta_2}, \quad 2\Delta_{6v} \equiv 2 \cos \lambda \equiv \left(\frac{w_2}{w_1^2} - 1 \right)^{-1}. \quad (6.6)$$

This form guarantees that the “two-interface scattering” is consistent, or

$$\begin{aligned} (w_2 - w_1^2) g(n_j \rightarrow n, n_{j+1} \rightarrow n) - w_1 \bar{w}_1 g(n_j \rightarrow n+1, n_{j+1} \rightarrow n) \\ + (\bar{w}_2 - \bar{w}_1^2) g(n_j \rightarrow n+1, n_{j+1} \rightarrow n+1) = 0, \\ \text{for } j = 1, \dots, r-1. \end{aligned} \quad (6.7)$$

One can next verify that three-interface and higher scattering processes are consistent because of the special form (2.59), which relates to weights of fusion models generated from the six-vertex model.⁽⁶²⁾ This is also true for the case with $\Lambda \neq \bar{\Lambda}$, for which (6.5) need be amended with trivial $\bar{\Lambda}/\Lambda$ powers which break the left-right symmetry.

In (6.5), the last line corresponds to the usual Bethe Ansatz,⁽¹²⁾ whereas the summations over the ε 's correspond to all waves reflected at the two boundaries. The coefficients are chosen such that the first “left” boundary condition,

$$g(m_1 = \frac{1}{2}, \dots, m_r | \zeta_1, \dots, \zeta_r) = 0, \quad (6.8)$$

is automatically satisfied.

In order to solve the other “right” boundary condition

$$g(m_1, \dots, m_r = L + \frac{1}{2} | \zeta_1, \dots, \zeta_r) = 0, \quad (6.9)$$

we have to require the ‘‘Bethe Ansatz equations’’

$$\zeta_k^{2L} \prod_{j \neq k} \left(A(\zeta_j, \zeta_k) A(\zeta_j^{-1}, \zeta_k) \right) = 1, \quad k = 1, \dots, r. \quad (6.10)$$

We need to solve these equations (6.10) in the thermodynamic limit $L \rightarrow \infty$ at finite r and substitute the solutions in (6.3) and (6.4).

The large- L solution giving the largest eigenvalue is

$$\zeta_j = \frac{\cos\left(\left(\frac{r}{2} - \left[\frac{j-1}{2}\right]\right)\lambda\right)}{\cos\left(\left(\frac{r}{2} - \left[\frac{j+1}{2}\right]\right)\lambda\right)}, \quad j = 1, \dots, r, \quad (6.11)$$

with $[x]$ the integer part of x . For even r (6.11) reduces to

$$r = 2s, \quad \zeta_{2j-1} = \zeta_{2j} = \frac{\cos\left((s-j+1)\lambda\right)}{\cos\left((s-j)\lambda\right)}, \quad j = 1, \dots, s, \quad (6.12)$$

whereas for odd r it reduces to

$$r = 2s + 1, \quad \zeta_{2j-1} = \zeta_{2j} = \frac{\cos\left((s-j+\frac{3}{2})\lambda\right)}{\cos\left((s-j+\frac{1}{2})\lambda\right)}, \quad j = 1, \dots, s, \\ \zeta_{2s+1} = 1. \quad (6.13)$$

From these results we immediately obtain (2.75) with $\bar{\sigma}_r$ given by the last member of (2.76). We see that we are precisely at the boundary where the ζ pairs change from complex conjugate pairs to unequal real pairs, which may be related to some pre-wetting phenomena on the integrable line.

7. NEW MODEL

There is already a great deal of exact results obtained for the chiral Potts models. Yet not much of this has been utilized. One of the reasons is that the temperature dependence in the integrable chiral Potts model, as given by (2.7) through (2.9) is not very transparent. It is rather vague what the critical temperature T_c is, thus making it harder to use the exactly known exponents and other results for $N \geq 4$.

Moreover, one would like to have a model which includes the chiral Potts model as a special case, yet not so general as (2.2) which has too many variables. Such a model, with $N \geq 3$, can be used to describe some interesting physical phenomena, such as commensurate-incommensurate phase transitions and wetting phenomena. It may not be exactly solvable in most regions. Hence, numerical studies would have to be done on it. However, the model may be in the same universality class as the integrable chiral Potts model, and may be more interesting for $N \geq 4$ than the chiral clock model which has only a single cosine term in (2.12).

7.1. New 2-Parameter Chiral Potts Model for General N

We therefore propose a new model with nearest-neighbor pair interactions given by

$$-\mathcal{E}(n) = E \sum_{j=1}^{N-1} \frac{\sin(\pi/N)}{\sin(\pi j/N)} \cos\left(\frac{2\pi}{N}(nj + (N-2j)\Delta)\right). \quad (7.1)$$

This has only two variables E and Δ . For $\Delta = \frac{1}{4}$, it is identical with the pair-interaction energy (5.10) of the integrable chiral Potts model at zero temperature and is thus on the superwetting line there. For $\Delta \sim 0$, we find $\mathcal{E}(0)$ is the ground state. In fact, it is easy to show that for $\Delta < \Delta_{\text{CI}}$, with

$$\Delta_{\text{CI}} \equiv \frac{1}{4} \frac{(N+1)}{(N-1)}, \quad (7.2)$$

and at low temperatures the system is in the ferromagnetic phase (or $W(0)$ is the maximum). Within this regime, for $\Delta < \frac{1}{4}$, the system is unwetted, namely $\epsilon_p + \epsilon_{r-p} > \epsilon_r$; at $\Delta = \frac{1}{4}$, it goes through a superwetting transition, with $\epsilon_p + \epsilon_{r-p} = \epsilon_r$; while for $\Delta > \frac{1}{4}$, the system is wet, with $\epsilon_p + \epsilon_{r-p} < \epsilon_r$. At $\Delta = \Delta_{\text{CI}}$, we find that $\mathcal{E}(0) = \mathcal{E}(-1)$ as in the chiral clock model.^(50,54) Therefore, the ground state is highly degenerate and we believe that, at this point, the system goes through a commensurate-incommensurate phase transition.

7.2. Superwetting and Ground-State Degeneracy for $N=5$

To make all these statements clearer, let us take $N = 5$ as an illustration. We plot, in Fig. 12, the energy $\mathcal{E}(n)$ given in (7.1) as a function of $x = n/N$, for different values of Δ .

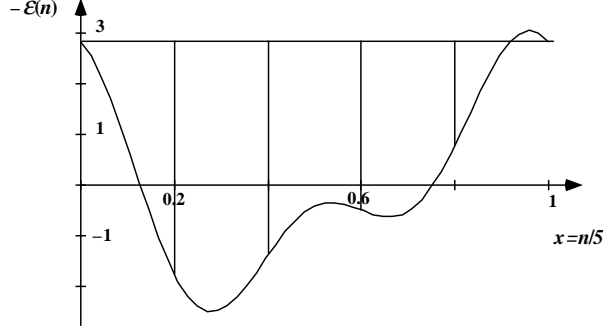


Fig. 12a. Energy $-\mathcal{E}(n)$ (or interfacial tension at zero temperature) versus $x = n/N = n/5$ for the new model with $N = 5$ and $\Delta = \frac{1}{6}$: ground state in the “dry phase” as no wetting can take place.

In Fig. 12a, we show the situation for $\Delta = \frac{1}{6} < \frac{1}{4}$. We find that the increments in energy — or the interfacial tension at zero temperature — $\epsilon_r = \mathcal{E}(-r) - \mathcal{E}(0)$ are given by

$$\begin{aligned} \epsilon_4 &= 4.574329190, & \epsilon_3 &= 4.209056927, \\ \epsilon_2 &= 3.315920618, & \epsilon_1 &= 2.036147842 \end{aligned} \quad (7.3)$$

and are shown in Fig. 12a as the lengths of vertical straight lines indicating the energy differences between the $\mathcal{E}(-r)$ and the ground state energy $\mathcal{E}(0)$. By examining the lengths of these straight lines, we find that $\epsilon_p + \epsilon_{r-p} > \epsilon_r$. Therefore it is energetically unfavorable to have two interfaces with interfacial tensions ϵ_p and ϵ_{r-p} instead of one with ϵ_r . Hence, the system is not wetted.

In Fig. 12b, we plot the energy \mathcal{E} for $\Delta = \frac{1}{4}$, and we find $\epsilon_r = r\epsilon_1 = 2r \sin \pi/5$. This means that it is energetically neutral to have one interface with ϵ_r or more than one, even r interfaces with ϵ_1 . This is what we have called superwetting.

In Fig. 12c, we plot \mathcal{E} for $\Delta = \frac{3}{10} > \frac{1}{4}$. We now find

$$\begin{aligned} \epsilon_4 &= 4.655997407, & \epsilon_3 &= 2.965539502, \\ \epsilon_2 &= 1.703676245, & \epsilon_1 &= 0.6789144637 \end{aligned} \quad (7.4)$$

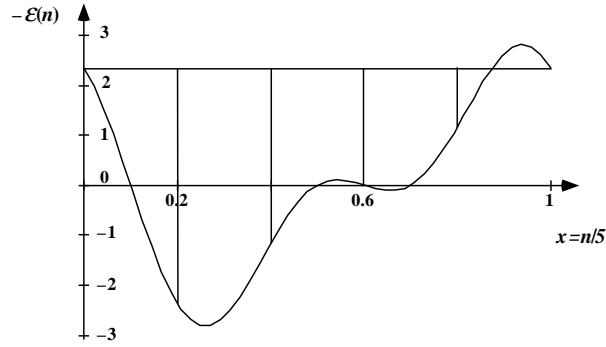


Fig. 12b. Energy $-\mathcal{E}(n)$ for $N = 5$ and $\Delta = \frac{1}{4}$: the ground-state is at a (super)wetting transition.

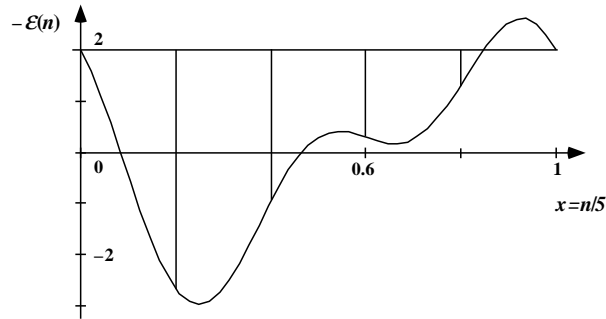


Fig. 12c. Energy $-\mathcal{E}(n)$ for $N = 5$ and $\Delta = \frac{3}{10}$: ground state in the wet phase.

and also that $r\epsilon_1 < \epsilon_p + \epsilon_{r-p} < \epsilon_r$. Consequently, it is energetically more favorable to have r interfaces with ϵ_1 than just one with ϵ_r or another number less than r . This means the system is wetted, allowing only one kind of interface with interfacial tension ϵ_1 .

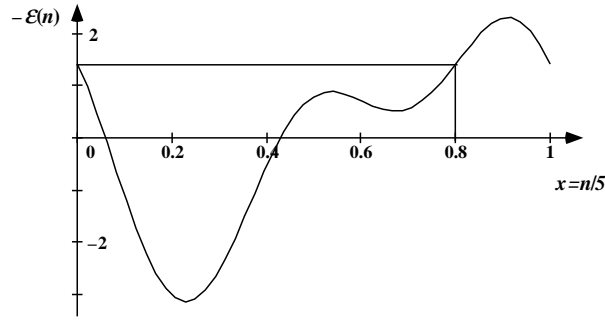


Fig. 13. Energy $-\mathcal{E}(n)$ for $N = 5$ and $\Delta = \frac{3}{8}$: the ground state is highly degenerate as $W(0) = W(N - 1)$ here.

We plot \mathcal{E} for $\Delta = \frac{3}{8}$ in Fig. 13, and we find $\mathcal{E}(N - 1) = \mathcal{E}(0)$. This is the same situation as in the chiral-clock model, namely that the ground state is highly degenerate for certain values of Δ . Hence, near $\Delta = \frac{3}{8}$ and at low temperature, there exist floating incommensurate phases. The model (7.1) can then be used to describe commensurate-incommensurate phase transitions. However, in these regimes, exact solutions do not exist and numerical methods have to be employed.

7.3. Comparison with Integrable Model for $N = 5$

Comparing with the values given by (5.4) for the integrable model, we find that the new model given by (7.1) is integrable at zero temperature at the special value $\Delta = \frac{1}{4}$. On the other hand, unlike for the new model, the ratios K_j/K_1 and Δ_j/Δ_1 for the integrable cases are not constants, as shown in Fig. 8 to Fig. 11. We believe that the new model may very well not be integrable at any other point. On the other hand, as the ratios for the

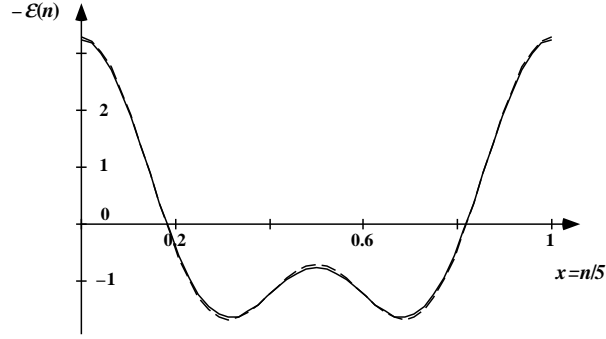


Fig. 14a. Comparison of the energies $-\mathcal{E}$ of the self-dual integrable chiral Potts model and the new model with $\Delta = 0$ for $N = 5$; the two curves are almost on top of each other.

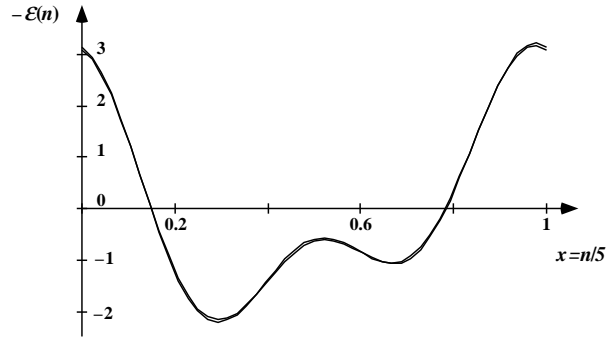


Fig. 14b. Comparison of the energies $-\mathcal{E}$ of the integrable chiral Potts and the new model at $\Delta = .0977875$ for $N = 5$; again the two curves are almost on top of each other.

integrable cases are almost constants, it is interesting to compare them. In Fig. 14a, we plot for $N = 5$ the nearest-neighbor interaction as a function of $x = n/N$ for the integrable case at the self-dual point with

$$\Delta_1 = \Delta_2 = 0, \quad K_1 = 1, \quad K_2/K_1 = 0.6409037097, \quad (7.5)$$

together with that of the new model at $\Delta = 0$. Also, in Fig. 14b, we plot the \mathcal{E} for the integrable model evaluated at $\theta = -9\pi/50$, with

$$\begin{aligned} \Delta_1 &= 0.2943916857, & \Delta_2 &= 0.09778750304, \\ K_1 &= 1, & K_2/K_1 &= 0.6404446571, \end{aligned} \quad (7.6)$$

and the $\mathcal{E}(n)$ of (7.1) evaluated at $\Delta = \Delta_2 = 0.09778750304$. We find that the curves are almost on top of each other.

As it is well known that by changing the strengths of the interactions, without changing the symmetry (here N) or spatial dimension, the exponents are universal, it is likely that the integrable model and the new model have the same critical exponents for the same N . On the other hand, the models must be different in some other sense and it would be interesting to find out more about them.

It may also be interesting to study variations of model (7.1), which agree with the symmetric integrable model at a non-zero temperature and to investigate if and how superwetting sets in. In the most general chiral Potts model there are enough parameters to allow the existence of solutions of the conditions for a superwetting line. It may be of interest to see, by low-temperature expansion for example, if there are solutions with real positive Boltzmann weights and what their physical implications are.

ACKNOWLEDGMENTS

We would like to thank Dr. A. J. Guttmann and Dr. W. Selke for their interest in the chiral Potts model and for stimulating discussions during the IUPAP conference in Berlin. We also like to thank Dr. B. M. McCoy for encouragement. We especially would like to thank Dr. R. J. Baxter for most helpful correspondence, which greatly enhanced our paper and helped us correcting some of our errors.

REFERENCES

1. L. Onsager, *Phys. Rev.* **65**:117 (1944).
2. L. Onsager, *Discussion, Nuovo Cimento*, ser. 9, **6** Suppl.:261 (1949).
3. L. Onsager, in *Critical Phenomena in Alloys, Magnets and Superconductors*, R. E. Mills, E. Ascher, and R. I. Jaffee, eds. (McGraw-Hill, New York, 1971), pp. xix–xxiv, 3–12.
4. B. Kaufman, *Phys. Rev.* **76**:1232 (1949).
5. B. Kaufman and L. Onsager, *Phys. Rev.* **76**:1244 (1949).
6. A. E. Kennelly, *Electrical World and Engineer* **34**:413 (1899).
7. J. B. McGuire, *J. Math. Phys.* **5**:622 (1964).
8. C. N. Yang, *Phys. Rev. Lett.* **19**:1312 (1967).
9. R. J. Baxter, *Exactly Solved Models in Statistical Mechanics* (Academic, London, 1982).
10. H. Au-Yang and J. H. H. Perk, in *Advanced Studies in Pure Mathematics*, Vol. 19 (Kinokuniya-Academic, Tokyo, 1989), p. 57.
11. V. G. Kac, in *Infinite Dimensional Lie Algebras* (Cambridge University Press, 1985).
12. H. Bethe, *Z. Phys.* **71**:205 (1931).
13. P. P. Kulish and E. K. Sklyanin, in *Integrable Quantum Field Theories*, J. Hietarinta and C. Montonen, eds. *Lecture Notes in Physics* **151** (Springer, Berlin, 1981), p. 61.
14. M. Jimbo, *Lett. Math. Phys.* **10**:63 (1985).
15. V. V. Bazhanov, *Phys. Lett. B* **159**:321 (1985).
16. V. G. Drinfel'd, in *Proceedings of the International Congress of Mathematicians* (Berkeley, Calif., 1986), p. 798.
17. L. D. Faddeev, N. Yu. Reshetikhin, and L. A. Takhtajan, in *Algebraic Analysis*, Vol. 1, M. Kashiwara and T. Kawai, eds. (Academic, San Diego, 1988), p. 129.
18. T. T. Wu, *Phys. Rev.* **149**:380 (1966).
19. L. P. Kadanoff, *Nuovo Cimento* **44B**:276 (1966).
20. M. E. Fisher and R. J. Burford, *Phys. Rev.* **156**:583 (1967).
21. T. T. Wu, B. M. McCoy, C. A. Tracy and E. Barouch, *Phys. Rev. B* **13**:316 (1976).
22. M. Sato, T. Miwa and M. Jimbo, *Proc. Japan Acad.* **53A**:6, 147, 153, 183 (1977).
23. J. H. H. Perk, *Phys. Lett. A* **79**:3 (1980).
24. E. H. Lieb, *Phys. Rev. Lett.* **18**:692 (1967).
25. E. H. Lieb and F. Y. Wu, in *Phase Transitions and Critical Phenomena*, Vol. 1, C. Domb and M. S. Green, eds. (Academic, London, 1972), p. 331.
26. G. von Gehlen and V. Rittenberg, *Nucl. Phys. B* **257** [FS14]:351 (1985).
27. L. Dolan and M. Grady, *Phys. Rev. D* **25**:1587 (1982).
28. J. H. H. Perk, in *Theta Functions Bowdoin 1987, Proc. Symp. in Pure Math.* Vol. 49 (Am. Math. Soc., Providence, RI, 1989).
29. B. Davies, *J. Math. Phys.* **32**:2945 (1991).
30. H. Au-Yang, B. M. McCoy, J. H. H. Perk, S. Tang, and M. L. Yan, *Phys. Lett. A* **123**:219 (1987).
31. R. J. Baxter, J. H. H. Perk, and H. Au-Yang, *Phys. Lett. A* **128**:138 (1988).

32. G. Albertini, B. M. McCoy, J. H. H. Perk, and S. Tang, *Nucl. Phys. B* **314**:741 (1989).
33. A. O. Morris, *Quart. J. Math. Oxford*, ser. 2, **18**:7 (1967); **19**:289 (1968).
34. A. J. Bracken and H. S. Green, *Nuovo Cimento* **9** A:349 (1972), and references quoted.
35. V. V. Bazhanov and Yu. G. Stroganov, *J. Stat. Phys.* **59**:799 (1990).
36. C. De Concini and V. G. Kac, in *Operator Algebras, Unitary Representations, Enveloping Algebras, and Invariant Theory*, A. Connes, M. Duflo, A. Joseph, and R. Rentschler, eds. (Birkhäuser, Boston, 1990), p. 471.
37. R. J. Baxter, *J. Stat. Phys.* **57**:1 (1989).
38. R. J. Baxter, *J. Stat. Phys.* **73**:461 (1993).
39. R. J. Baxter, *J. Phys. A* **27**:1837 (1994).
40. R. J. Baxter, *J. Stat. Phys.* **52**:639 (1988).
41. G. Albertini, B. M. McCoy, and J. H. H. Perk, in *Advanced Studies in Pure Mathematics*, Vol. 19 (Kinokuniya-Academic, Tokyo, 1989), p. 1.
42. R. B. Potts, *Proc. Camb. Phil. Soc.* **48**:106 (1952).
43. F. Y. Wu, *Rev. Mod. Phys.* **54**:235 (1982), **55**:315 (1983).
44. R. J. Baxter, *Exactly Solved Models in Statistical Mechanics* (Academic, London, 1982), pp. 322–351.
45. V. A. Fateev and A. B. Zamolodchikov, *Phys. Lett. A* **92**:37 (1982).
46. B. M. McCoy, J. H. H. Perk, S. Tang, and C. H. Sah, *Phys. Lett. A* **125**:9 (1987).
47. H. Au-Yang, B. M. McCoy, J. H. H. Perk, and S. Tang, in *Algebraic Analysis*, Vol. 1, M. Kashiwara and T. Kawai, eds. (Academic, San Diego, 1988), p. 29.
48. R. J. Baxter, *Phil. Trans. Roy. Soc. London Ser. A* **289**:315 (1978).
49. D. A. Huse, A. M. Szpilka, and M. E. Fisher, *Physica A* **121**:363 (1983).
50. W. Selke and J. M. Yeomans, *Z. Phys. B* **46**:311 (1982).
51. W. Selke and W. Pesch, *Z. Phys. B* **47**:335 (1982).
52. M. E. Fisher, *J. Stat. Phys.* **34**:667 (1984).
53. J. Yeomans and B. Derrida, *J. Phys. A* **18**:2343 (1985).
54. W. Selke, *Phys. Repts.* **170**:213 (1988).
55. A. L. Stella, X.-C. Xie, T. L. Einstein, and N. C. Bartelt, *Z. Phys. B* **67**:357 (1987).
56. R. B. Griffiths, in *Phase Transitions in Surface Films*, J. G. Dash and J. Ruvalds, eds. (Plenum, New York and London, 1980), p. 1, see particularly eq. (5.13) and surrounding text.
57. D. B. Abraham, L. F. Ko, and N. M. Švrakić, *Phys. Rev. B* **38**:12011 (1988), and references cited.
58. M. Gaudin, *La Fonction d'Onde de Bethe* (Masson, Paris, 1983).
59. A. N. Kirillov, *Zap. Nauch. Semin. LOMI* **164**:121 (1987) [*J. Sov. Math.* **47**:2450 (1989)].
60. W. Nahm, A. Recknagel, and M. Terhoeven, *Mod. Phys. Lett. A* **8**:1835 (1993).
61. M. den Nijs, *J. Phys. A* **17**:L295 (1984).
62. P. P. Kulish, N. Yu. Reshetikhin, and E. K. Sklyanin, *Lett. Math. Phys.* **5**:393 (1981).